Study on the Transport Phenomena in Complex Micro-Reactors

By Eric Mielke

Thesis submitted to the Faculty of Graduate and Postdoctoral Studies as required for the degree of Master of Applied Science

In

Department of Chemical and Biological Engineering
Faculty of Engineering

uOttawa

University of Ottawa

Abstract

Continuous processing in the pharmaceutical and fine chemical industries, particularly in micro/milli-scale reactors, has been a topic of interest in literature in recent years due to the advantages offered over batch reactions. One such advantage is the enhanced transport properties of operating at smaller scales, although the quantification of the transport phenomena is not straightforward when wall and entrance effects cannot be neglected.

In the first study presented, various micro-mixer geometries and scales were considered to increase the mixing efficiency in liquid-liquid systems of diverse interfacial tensions for fast reactions. The conditions were varied over different flow regimes; including slug flow, parallel flow, and drop flow. A mass-transfer-limited test reaction was used to evaluate the overall volumetric mass transfer coefficients ($K_{org}a$) as a function of the average rate of energy dissipation (ε) for each mixer design. The onset of drop flow occurred at a lower ε for the LL-Triangle mixer when compared with the Sickle or LL-Rhombus mixers for low interfacial-tension systems (i.e., n-butanol-water). In the drop flow regime for energy dissipation rates of around 20 to 500 W/kg, $K_{org}a$ values ranged from approximatively 0.14 to 0.35 s^{-1} and 0.004 to 0.015 s^{-1} for the relatively low and high interfacial-tension (i.e., toluene-water) systems, respectively.

The second investigation explored the heat transfer properties of a FlowPlate® system by Ehrfeld Mikrotechnik BTS. First, in a non-reactive system with rectangular serpentine channels ($d_h < 1mm$, $400 < Re < 2000$), a Gnielinski-type model was fit to the internal Nusselt number. Using a silver-based thermal paste between the reactor and heat transfer fluid plates proved to reduce the external resistance to heat transfer by ~70%, yielding overall heat transfer coefficients of ~2200 $[W/(m^2K)]$. Secondly, a Grignard reaction was highlighted as a test reaction to compare different reactors' localized heat transfer characteristics (i.e., hotspot formation) with various micro-mixer geometries, materials, injection ports, and channel scales. Lastly, a case study of four reactions utilized the fourth Damköhler number to determine a maximum channel diameter that would remove sufficient heat to avoid hotspot formation.

Each of these studies provides insight to aid in the proper selection of a reactor for a given set of physical properties and reaction kinetics/enthalpies.

Résumé

La production en continue dans les industries pharmaceutiques et chimie fine, en particulier dans les réacteurs micro/milli-échelle, a été un sujet d'intérêt dans la littérature ces dernières années en raison des avantages relatifs aux procédés en cuvés. Un des avantages réside dans les propriétés de transport améliorés en opérant à des échelles plus petites, bien que la quantification des phénomènes d'échange ne soit pas simple lorsque les effets de paroi et d'entrée ne peuvent être négligés.

Dans la première étude présentée, diverses géométries et échelles de micro-mélangeurs ont été considérées pour améliorer l'efficacité de mélange dans des systèmes liquide-liquide de tensions interfaciales variés pour des réactions rapides. Les conditions d'opérations ont été variées afin d'obtenir différents régimes d'écoulement; Y compris l'écoulement piston, l'écoulement parallèle et l'écoulement en gouttes dispersées. Une réaction test limitée par le transfert de masse a été utilisée pour évaluer les coefficients volumétriques globaux de transfert de masse ($K_{org}a$) en fonction du taux moyen de dissipation d'énergie (ε) pour chaque type de mélangeur. Le début du régime d'écoulement en gouttes dispersées s'est produit à un ε inférieur pour le mélangeur LL-Triangle par rapport aux mélangeurs Sickle ou LL-Rhombus pour des systèmes à faible tension interfaciale (c'est-à-dire n-butanol-eau). Dans le régime d'écoulement en gouttes dispersées, pour des taux de dissipation d'énergie d'environ 20 à 500 W/kg, les valeurs de $K_{org}a$ variaient approximativement de 0,14 à 0,35 s^{-1} et 0,004 à 0,015 s^{-1} pour les systèmes à tension interfaciale relativement basse et élevée (c'est-à-dire toluène-eau), respectivement.

La deuxième étude a exploré les propriétés de transfert de chaleur d'un système FlowPlate® par Ehrfeld Mikrotechnik BTS. Tout d'abord, dans un système non réactif avec des canaux rectangulaires en serpentin (d_h <1mm, 400 <Re <2000), un modèle de type Gnielinski a été adapté au nombre de Nusselt interne. L'utilisation d'une pâte thermique à base d'argent entre le réacteur et les plaques de fluide caloporteur a permis de réduire la résistance externe au transfert de chaleur de ~70%, ce qui donne des coefficients globaux de transfert de chaleur de ~2200 [$W/(m^2K)$]. Deuxièmement, une réaction de Grignard a été mise en évidence comme réaction test pour comparer les caractéristiques de transfert de chaleur localisées (c'est-à-dire la formation de points chauds) de différents réacteurs avec diverses géométries, matériaux, points d'injection et échelles du canal. Enfin, une étude de cas de quatre réactions a utilisé le quatrième nombre de Damköhler

pour déterminer un diamètre de canal maximal qui éliminerait suffisamment de chaleur pour éviter la formation de points chauds.

Chacune de ces études fournit des informations pour aider à la sélection appropriée d'un réacteur pour un ensemble donné de propriétés physiques et de cinétiques/enthalpies de réaction.

Declaration of Contributors

I hereby declare that I am the sole author of this thesis. My supervisors, Arturo Macchi and Dominique Roberge, provided comments and corrections throughout my work.

All the experiments of Sections 2 were designed by myself while at the R&D laboratories of Lonza AG. The experiments were performed by myself or with the help of Chistof Aellig, and Tobias Federer, employees at Lonza.

All the results of Section 3.2.1 were obtained by myself at the University of Ottawa with the help of Nikhil Koushik who is acknowledged as a co-author. The results from section 3.2.2 were initially collected by Markus Eyholzer and Michael Gottsponer (acknowledged as co-authors). Norbert Kockmann designed the SiC microreactor (acknowledged as co-author), and the analysis and discussion were performed by myself with the direction of my supervisors. Dr. Patrick Plouffe provided guidance in the analysis of section 3.2.3 and is listed as co-author as well.

All the presented data analysis and modeling were performed by myself only.

Acknowledgements

I would first like to thank my supervisors, Dr. Arturo Macchi and Dr. Dominique Roberge for their dedicated support and guidance over the past two years. They could always provide new, unique approaches to a problem whenever I was stuck, and their direction is a key factor in my success. I also want to thank my friends and colleagues Dr. Patrick Plouffe for his mentorship and guidance when I was starting my degree, and Valois Parisien for when I needed a fresh set of eyes to look at my analysis.

I want to acknowledge the financial support of Lonza AG, of the Natural Sciences and Engineering Research Council of Canada (NSERC) IPS, of the NSERC Continuous Flow CREATE program, and of the University of Ottawa.

I am grateful for my friends and classmates who helped make my time at uOttawa and Visp, Switzerland unforgettable and enjoyable. Finally, I would like to thank my family, particularly my fiancé Megan Young, for their continued love and support throughout my studies.

Table of Contents

List of Figures

List of Tables

1. Introduction

1.1. Background

In pharmaceutical and fine chemical industries, there has been an increased interest in the development of continuous flow processes in micro-reactors, over batch-wise systems [1–4]. This trend stems from the relative ease in scale-up of flow systems, the potential for process intensification due to operation at small scales, increased process safety in handling hazardous materials, and the increased rates of transport.

As there are several stages in the development of new pharmaceutical chemicals, each requiring increased campaign sizes [5,6], micro-reactors offer added flexibility in their scale-up than in batch systems. Since it is possible to maintain mixing properties for single-phase [7] and multi-phase [8] systems at a given rate of energy dissipation (ε), the channel size can be increased such that a given increase in flow will yield the same ε. As a proof of concept, this strategy was employed for a mixing-limited lithiation reaction where similar yields were obtained in separate reactors, one with double the hydraulic diameter of the other, where over 2 tons of isolated material was produced [3].

Process intensification is a clear advantage of micro-reactors [3,4,7,9–12]. With smaller channel sizes, it is possible to operate at higher pressures, and therefore temperatures (due to increased boiling point of the solvent). Higher temperatures allow for faster reaction kinetics, while higher pressures give higher gas concentrations in gas-liquid systems. These factors lead micro-reactors to increase the space-time yield by orders of magnitude when compared to batch reactors [13]. Additionally, it is possible to perform hazardous reactions, such as oxidations with pure O_2 [14,15], in a safer manner. In flow, multistep reactions involving highly explosive intermediates can be performed continuously without the isolation of dangerous materials, such as diazo compounds [12,16,17].

The last main advantage to micro-reactor technology is the improved transport phenomena with smaller length scales. Micro-reactors offer a variety of mixing strategies for single phase or multiphase; either through passive [18] (e.g., obstacles, curvature in the channels, etc.) or active [19,20] (e.g., pulsating flow, ultrasound, magnetic stirrers, etc.) mixing techniques. Various passive mixing structures have been studied extensively in single-phase [3,4,7,9–12] and multi-

phase systems [2,12,18,21,22] and have been found to have mixing times up to 2 orders of magnitude faster than larger scale reactors [10]. In addition to the improved hydrodynamics, micro-channels also have intrinsically higher surface-area-to-volume ratios for heat transfer which can exchange sufficient heat for highly exothermic/endothermic reactions. In multi-phase systems, the small channel sizes (and mixing strategies previously mentioned) allow for smaller droplets to form, increasing the interfacial area available for mass exchange [18,23].

1.2. Motivation and Research Topics

While there are many different micro-reactor systems available commercially from companies such as ThalesNano Inc, Ehrfeld Mikrotechnik BTS, Syrris Ltd, Vapourtec Ltd, etc., it is important to use the proper system for a given application. For this reason, Plouffe et al. [24] developed a "toolbox" which could be used to select a reactor type effectively. Reactive systems were divided into reaction types based on their kinetics/thermal requirements, as well as the phase system (homogenous, liquid-liquid, liquid-gas, gas-solid, etc.). The objective of this work is to study and better define the transport phenomena for certain "tools" in the toolbox; namely mixer geometries for fast (type A) liquid-liquid reactions, and heat transfer properties of micro-reactors for homogenous systems.

1.3. Thesis Outline

Section 2 investigates several micro-mixer geometries which were developed in order to improve the mixing efficiency for fast liquid-liquid reactions based on previous work by Plouffe et al. [18]. It has been published under the title "**Microreactor mixing-unit design for fast liquid-liquid reactions**". Various flow regimes (slug flow, parallel flow, and drop flow) were investigated visually and with a test reaction, the two-phase hydrolysis of 4-nitrophenyl acetate in sodium hydroxide solution, to analytically measure the overall volumetric mass transfer coefficients ($K_{org}a$) as a function of the average rate of energy dissipation (ε) for the different mixer designs and flow regimes. These were compared with different solvent-pairs to consider the effect of interfacial tension on the onset of drop flow.

Section 3 was focused on single-phase heat transfer in micro-channels, and the results will be submitted for publication under the title "**Investigation of Overall and Localized Heat Transfer in Curved Micro-Channel Reactor Systems**". Using the FlowPlate® system by Ehrfeld

Mikrotechnik BTS, heat transfer experiments with a reactive and non-reactive systems were performed. For a range of Reynolds numbers between 400-2000, a Gnielinski-type model was used to fit the Nusselt number results in the non-reactive system. In the reactive system, the fast and highly exothermic synthesis of methyl 2-oxobutanoate, using dimethyl-oxalate and the Grignard reagent ethylmagnesium chloride, was studied. Due to the selectivity's temperature dependence, this proved to be a sensitive test reaction to differentiated the localized heat transfer characteristics in various reactor sizes, injection modes, geometries, and wall materials. Lastly, four reaction systems were analyzed in a case study based on the fourth Damköhler number to calculate the maximum channel size that can remove sufficient heat to avoid a hotspot from the enthalpy of reaction.

In conclusion, the each of the two sections aid in the selection and sizing of a micro-reactor system for mass-transfer-limited liquid-liquid systems or systems which require significant heat transfer, as summarized in section 4. Recommendations for future work are also provided in order to extend the scope of this project.

1.4. Other Considerations in the Study of Heat Transfer in Microreactors

In the literature for heat transfer studies in micro-reactors and micro-channels, there is no strong consensus regarding the application of conventional, macro-scale correlations to micro-scale channels, as there is significant variance in the observed results [25–28]. Steinke and Kandlikar considered three key, underlying causes specific to research in micro-reactor systems responsible for the differences in various investigations [25,28]. These were taken into account when choosing the operating conditions for Section 3:

i) *Thermal Entrance Length*: Micro-channels generally have shorter relative lengths (l/D_h) that are often employed to reduce the total pressure drop. Both the hydrodynamic and thermally developing regions can represent a larger fraction of the total length, and the local heat transfer coefficient is higher in this region than the fully developed region [25]. The fluid is often considered to be thermally developed after a certain length, L_t, defined by equation (1.1) for laminar flow in a straight channel [25]. Where Re is the Reynolds number (ratio of inertial to viscous forces), and Pr is the Prandtl number (ratio of momentum to thermal diffusivities). The value of the constant,

c, often ranges between 0.05 and 0.1 [25], but was shown to be closer to 0.02 when rectangular ducts with aspect ratios (α) of 10 or more were used [29]. This leads to the thermal entrance length accounting for between 5-15% of the overall reactor length for the conditions studied, where the channel's aspect ratio was 10.

$$\frac{L_t}{D_h} = cRePr \tag{1.1}$$

ii) *Uncertainties in Experimental Measurements*: Steinke and Kandlikar defined the overall uncertainty in the Nusselt number calculation, δ_{Nu}, and the terms relevant to the system studied here are shown in equation (1.2).

$$\delta_{Nu} = Nu \cdot \left[\left(\frac{\delta_{k_f}}{k_f}\right)^2 + 4\left(\frac{\delta_{T_s}}{T_s}\right)^2 + 2\left(\frac{\delta_{T_{c,i}}}{T_{c,i}}\right)^2 + 2\left(\frac{\delta_{T_{c,o}}}{T_{c,o}}\right)^2 + 3\left(\frac{\delta_l}{l}\right)^2 + 5\left(\frac{\delta_w}{w}\right)^2 + 4\left(\frac{\delta_d}{d}\right)^2\right]^{1/2} \tag{1.2}$$

Where k_f is the fluid's thermal conductivity, T_s is the wall surface temperature, and $T_{c,i}$ and $T_{c,o}$ are the fluid inlet and outlet temperatures, respectively. Lastly, l, w, and d are the channel's length, width, and depth, respectively. To minimize the uncertainty, it is not only important to measure the temperature accurately, but also ensure that the outlet temperature is not too close to thermal equilibrium with the jacket temperature. In addition, the channel dimensions must be well known, as this plays a large role in the overall uncertainty.

iii) *Ambiguity in the Determination of the Thermal Boundary Condition*: Micro-channels can have complex boundary conditions which greatly change the theoretical predictions. A constant heat flux can be assumed when a fluid is heated from an electrical source (e.g., a microchip, or electrical heater), while a circumferentially and axially constant wall temperature is assumed for phase changes or reactions at a given temperature. Often the actual boundary condition can lie between a constant flux and constant wall temperature [25]. In order to assume a constant wall temperature, the jacket heat transfer fluid used in this work was kept at a high flow such that it enters and exits with minimal loss of temperature.

It is also important to consider the various walls of the channel. Some micro-reactor systems have one side insulated with silicon or glass plates; while others have thin walls between the channels which act more like fins with a fin efficiency that must be taken into account. When numerically

solving heat transfer problems in reactors with walls between the channels, the walls can often be considered one dimensional for the purposes of conduction [30].

1.5. Nomenclature

Symbols		$[Units]$
General		
a	Specific area (single phase) or specific interfacial area (biphasic)	$[m^2/m^3]$
c	Empirical constant for calculation of thermal developing region	$[-]$
d	Contraction depth	$[m]$
D_h	Hydraulic diameter at contraction $(2wd/(w+d))$	$[m]$
k	Thermal conductivity	$[W/(m\,K)]$
K_{org}	Overall convective mass transfer coefficient (m/s)	$[m/s]$
l	Reactor Length	$[m]$
L_t	Length of thermal developing region	$[m]$
Nu	Nusselt Number	$[-]$
Pr	Prandtl Number	$[-]$
Re	Reynolds Number	$[-]$
T	Temperature	$[°C\ or\ K]$
w	Contraction width	$[m]$
Greek Symbols		
α	Aspect ratio (w/d)	$[-]$
δ_x	Uncertainty with respect to value of any parameter, x	$[-]$
ε	Average rate of energy dissipation $(\Delta P/\rho\tau)$	$[m^2/s^3]$
Subscript		
c	Cold stream	
f	Fluid	
i	Measured at inlet	
o	Measured at outlet	
s	Conditions at the wall surface	

1.6. References

[1] N.-T. Nguyen, Z. Wu, Micromixers—a review, J. Micromechanics Microengineering. 15 (2005) R1–R16. doi:10.1088/0960-1317/15/2/R01.

[2] M.N. Kashid, L. Kiwi-Minsker, Microstructured Reactors for Multiphase Reactions: State of the art, Ind. Eng. Chem. Res. 48 (2009) 6465–6485. doi:10.1021/ie8017912.

[3] N. Kockmann, M. Gottsponer, D.M. Roberge, Scale-up concept of single-channel microreactors from process development to industrial production, Chem. Eng. J. 167 (2011) 718–726. doi:10.1016/j.cej.2010.08.089.

[4] V. Kumar, M. Paraschivoiu, K.D.P. Nigam, Single-phase fluid flow and mixing in microchannels, Chem. Eng. Sci. 66 (2011) 1329–1373. doi:10.1016/j.ces.2010.08.016.

[5] L. Malet-Sanz, F. Susanne, Continuous flow synthesis. a pharma perspective, J. Med. Chem. 55 (2012) 4062–4098. doi:10.1021/jm2006029.

[6] N. Kockmann, M. Gottsponer, B. Zimmermann, D.M. Roberge, Enabling continuous-flow chemistry in microstructured devices for pharmaceutical and fine-chemical production, Chem. - A Eur. J. 14 (2008) 7470–7477. doi:10.1002/chem.200800707.

[7] C.P. Holvey, D.M. Roberge, M. Gottsponer, N. Kockmann, A. Macchi, Pressure drop and mixing in single phase microreactors: Simplified designs of micromixers, Chem. Eng. Process. Process Intensif. 50 (2011) 1069–1075. doi:10.1016/j.cep.2011.05.016.

[8] P. Plouffe, M. Bittel, J. Sieber, D.M. Roberge, A. Macchi, On the scale-up of micro-reactors for liquid–liquid reactions, Chem. Eng. Sci. 143 (2016) 216–225. doi:10.1016/j.ces.2015.12.009.

[9] P. Plouffe, R. Anthony, A. Donaldson, D.M. Roberge, N. Kockmann, A. Macchi, Transport Phenomena in Two-Phase Liquid-Liquid Micro-Reactors, in: ASME 2012 10th Int. Conf. Nanochannels, Microchannels, Minichannels, Rio Grande, Puerto Rico, 2012. http://proceedings.asmedigitalcollection.asme.org/proceeding.aspx?articleid=1719073 (accessed August 19, 2014).

[10] M. Kashid, A. Renken, L. Kiwi-Minsker, Mixing efficiency and energy consumption for five generic microchannel designs, Chem. Eng. J. 167 (2011) 436–443. doi:10.1016/j.cej.2010.09.078.

[11] L. Falk, J.M. Commenge, Performance comparison of micromixers, Chem. Eng. Sci. 65 (2010) 405–411. doi:10.1016/j.ces.2009.05.045.

[12] V. Hessel, D. Kralisch, N. Kockmann, T. Noel, Q. Wang, Novel Process Windows for Enabling, Accelerating, and Uplifting Flow Chemistry, ChemSusChem. 6 (2013) 746–789. doi:10.1002/cssc.201200766.

[13] V. Hessel, Process windows - gate to maximizing process intensification via flow chemistry, Chem. Eng. Technol. 32 (2009) 1655–1681. doi:10.1002/ceat.200900474.

[14] B. Gutmann, P. Elsner, D.P. Cox, U. Weigl, D.M. Roberge, C.O. Kappe, Toward the synthesis of noroxymorphone via aerobic palladium-catalyzed continuous flow n-demethylation strategies, ACS Sustain. Chem. Eng. 4 (2016) 6048–6061. doi:10.1021/acssuschemeng.6b01371.

[15] C.A. Hone, D.M. Roberge, C.O. Kappe, The Use of Molecular Oxygen in Pharmaceutical Manufacturing: Is Flow the Way to Go?, ChemSusChem. (2016) 1–11. doi:10.1002/cssc.201601321.

[16] L.J. Martin, A.L. Marzinzik, S. V. Ley, I.R. Baxendale, Safe and reliable synthesis of

diazoketones and quinoxalines in a continuous flow reactor, Org. Lett. 13 (2011) 320–323. doi:10.1021/ol1027927.

[17] X. Zhang, S. Stefanick, F.J. Villani, Application of Microreactor Technology in Process Development, Org. Process Res. Dev. 8 (2004) 455–460. doi:10.1021/op034193x.

[18] P. Plouffe, D.M. Roberge, A. Macchi, Liquid–liquid flow regimes and mass transfer in various micro-reactors, Chem. Eng. J. 300 (2016) 9–19. doi:10.1016/j.cej.2016.04.072.

[19] S.S. Mongeon, D.M. Roberge, M. Bittel, P. Elsner, A. Macchi, Liquid–Liquid Mass Transfer in an Oscillatory-Flow Mesoscale Coil Reactor without Baffles, Org. Process Res. Dev. (2016) acs.oprd.5b00356. doi:10.1021/acs.oprd.5b00356.

[20] H. Monnier, A.M. Wilhelm, H. Delmas, Effects of ultrasound on micromixing in flow cell, Chem. Eng. Sci. 55 (2000) 4009–4020. doi:10.1016/S0009-2509(00)00067-1.

[21] L. Ducry, D.M. Roberge, Controlled Autocatalytic Nitration of Phenol in a Microreactor, Angew. Chemie - Int. Ed. 44 (2005) 7972–7975. doi:10.1002/anie.200502387.

[22] G. Dummann, U. Quittmann, L. Gröschel, D.W. Agar, O. Wörz, K. Morgenschweis, The Capillary-Microreactor: A New Reactor Concept for the Intensification of Heat and Mass Transfer in Liquid-Liquid Reactions, Catal. Today. 79–80 (2003) 433–439. doi:10.1016/S0920-5861(03)00056-7.

[23] P. Plouffe, D.M. Roberge, J. Sieber, M. Bittel, A. Macchi, Liquid–liquid mass transfer in a serpentine micro-reactor using various solvents, Chem. Eng. J. 285 (2016) 605–615. doi:10.1016/j.cej.2015.09.115.

[24] P. Plouffe, A. Macchi, D.M. Roberge, From Batch to Continuous Chemical Synthesis—A Toolbox Approach, Org. Process Res. Dev. (2014). doi:10.1021/op5001918.

[25] S. Kandlikar, S. Garimella, D. Li, S. Colin, M.R. King, Heat Transfer and Fluid Flow in Minichannels and Microchannels, 2nd ed., Elsevier Ltd., Kidlington, Oxford, 2014. doi:10.1016/B978-0-08-098346-2.00003-X.

[26] F.P. Incropera, D.P. DeWit, T.L. Bergman, A.S. Lavine, Fundamentals of Heat and Mass Transfer, 7th ed., John Wiley & Sons, Inc., Jefferson City, 2011.

[27] G.L. Morini, Single-phase convective heat transfer in microchannels: A review of experimental results, Int. J. Therm. Sci. 43 (2004) 631–651. doi:10.1016/j.ijthermalsci.2004.01.003.

[28] M.E. Steinke, S.G. Kandlikar, Single-phase liquid heat transfer in microchannels, in: 3rd Int. Conf. Microchannels Minichannels, 2005. doi:10.1115/ICMM2005-75114.

[29] P.S. Lee, S. V. Garimella, Thermally developing flow and heat transfer in rectangular microchannels of different aspect ratios, Int. J. Heat Mass Transf. 49 (2006) 3060–3067. doi:10.1016/j.ijheatmasstransfer.2006.02.011.

[30] P.S. Lee, S. V. Garimella, D. Liu, Investigation of heat transfer in rectangular microchannels, Int. J. Heat Mass Transf. 48 (2005) 1688–1704. doi:10.1016/j.ijheatmasstransfer.2004.11.019.

2. Micro-Reactor Mixing-Unit Design for Fast Liquid-Liquid Reactions

Eric Mielke,[a] Dominique M. Roberge,[b] and Arturo Macchi[a]

a, Centre for Catalysis Research and Innovation, Department of Chemical and Biological Engineering, University of Ottawa, K1N 6N5 Ottawa, Canada.

b, Chemical Manufacturing Technologies, Lonza AG, CH-3930 Visp, Switzerland.

This manuscript has been published J. Flow Chem. 2016, 6(3), 279–287

ABSTRACT

Based on previous work studying complex micro-reactors, it was desired to further improve the mixing efficiency by varying the mixing unit design for fast liquid-liquid reactions. Different flow regimes were studied; including slug flow, parallel flow, and drop flow. The two-phase hydrolysis of 4-nitrophenyl acetate in sodium hydroxide solution was used to evaluate the overall volumetric mass transfer coefficients ($K_{org}a$) as a function of the average rate of energy dissipation (ε) for each micro-reactor design and all flow regimes. The liquid-liquid systems investigated used n-butanol or toluene as the organic phase solvent and a 0.5 M NaOH aqueous solution. The use of surfactant was also investigated with the *toluene-water* system. All micro-reactor geometry designs were based on contraction-expansion repeating units with asymmetric obstacles to aid the breakup of slugs, and desynchronize the recombination of split streams. The investigated designs were chosen to avoid the formation of the parallel flow regime; contrary to curvature-based mixing-unit designs. The micro-reactor design can then be optimized to reduce the ε required to reach drop flow, since $K_{org}a$ has been found to be constant at equal ε for a given solvent system in this flow regime, regardless of the reactor selection. Additionally, the "$3/7^{th}$" scale-up rule was applied and confirmed with the LL-Triangle mixer. It was found that for low interfacial-tension systems (i.e., n-butanol-water), the onset of drop flow occurred at a lower ε for the LL-Triangle mixer when compared with the Sickle or LL-Rhombus mixers.

Keywords: Micro-reactor, Liquid-liquid reaction, Mass transfer, Mixing, Slug- Parallel- drop- and dispersed-flow

2.1. Introduction

In the past 10 years, flow technologies have become an ever more popular field of study in the fine chemical and pharmaceutical industries[1]. Continuous-flow is an attractive alternative to conventional batch processing with a number of benefits; namely process intensification via higher operating pressures and temperatures, and the increased surface-to-volume ratios involved with miniaturization (micro-reactors). While these advantages have been studied extensively in single phase systems[1–7], much of the research on multiphase systems[7–10] involves slug or parallel flow regimes where interphase mass transfer is relatively slow.

Previous work[11–17] studied the effects of using passive micro-mixing structures to increase the mass transfer rate between two immiscible phases in flow ranges that would have otherwise been in the slug flow regime for a similar-sized capillary reactor. A micro-mixer-based reactor was shown to be well suited for fast liquid-liquid reactions[14] (i.e., mass or heat transfer limited with reaction times in the millisecond to second range). Plouffe et al. further investigated the dependency of flow regimes on solvent-pair selection[12] and micro-mixer structure[11]. It was found that systems with low interfacial tension could transition from slug, to parallel, and then to drop flow regime with increasing flow rates; whereas systems with higher interfacial tension would not favour the parallel flow regime to form. Slug flow was shown to have an increasing overall volumetric mass transfer coefficient ($K_{org}a$) with flow while the transition from slug to parallel flow would cause a significant drop in $K_{org}a$ due to the decreased surface area available for interphase mass transfer. The drop flow regime was found to have the highest $K_{org}a$ and would only increase with flow. In the study involving various reactor geometries[11], it was also shown that $K_{org}a$ is only a function of the average rate of energy dissipation (ε) and solvent-pair once the flow has reached the drop flow regime, independent of reactor geometry, indicating that an ideal micro-mixer for fast liquid-liquid reactions must achieve drop flow at the lowest possible ε.

While investigating various mechanisms of mixing in micro-mixer, it was found that curvature-based micro-mixers could allow for the formation of a parallel flow regime while this was avoided in obstacle-based micro-mixers. Parallel flow is caused by the difference in densities between the two phases; where the denser phase would be forced to the outer edge of the curve due to centrifugal forces. When an increased rate of interphase mass transfer is desired, parallel flow

should be avoided due to the reduced internal circulation in each phase, along with the reduced specific area available for mass transfer when compared with slug or drop flow regimes.

This work investigates the LL-Rhombus and LL-Triangle micro-mixers, which are designed as modifications to the Sickle mixer with reduced curvature while keeping a contraction-expansion and obstacle as primary modes of energy dissipation. The only difference between the LL-Rhombus and LL-Triangle (which is shown in Figure 2.1) is the obstacle shape; where the rhombus has a more hydrodynamic shape with a cutting angle of 42°, whereas the triangle has an abrupt wall at a 90° angle towards the flow direction. The use of an obstacle with an angle greater than 90° and reverting flow in the opposite direction[18] was avoided as it could generate parallel flow under some conditions[11]. Another LL mixer without obstacle was tested to confirm that an obstacle is beneficial for more efficient mixing than solely relying on the contraction-expansion.

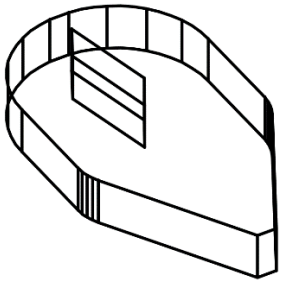

Figure 2.1. 3D visualization of the LL-Rhombus mixing element

2.2. Experimental

The experimental and HPLC analytical methods used are similar to those used in previous work by Plouffe et al.[11–13] with differences in the specific reactor plates and solvents used. The specifications for the specific reactor plates can be found in Table 2.2 and Table 2.3.

2.2.1. Equipment Setup

2.2.1.1. Size 600 Experimental Setup

For the size 600 tests, the Ehrfeld MMRS was used with Lonza FlowPlate® Lab reactors made from either stainless steel 316 or Hastelloy C22™. The setup can be seen in Figure 2.2. The system was fed the aqueous and organic solutions using two Syrdos (HiTec Zang) pumps with 5 or 2.5 mL syringes. Endress-Hauser Coriolis flow meters were used to measure the mass flow rates, and 25 or 6 bar Wika M-11 pressure transducers measured the pressure difference from the inlet to the

outlet of the reactor. The system was kept at ambient temperatures using a Huber Ministat 125 thermal bath.

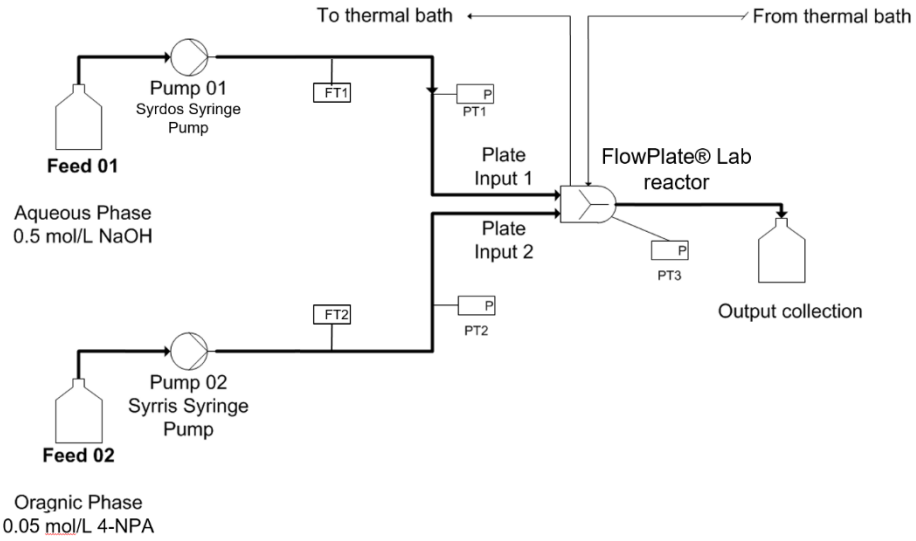

Figure 2.2. Size 600 micro-reactor experimental setup

2.2.1.2. Size 300 Experimental Setup

The setup for the size 300 scaled-up mixers was identical for the size 600, except Ismatec Reglo-Z gear pumps were used for the higher flow rates.

2.2.1.3. Solvent Systems

The physical properties of the aqueous and organic phases used can be found in Table 2.1. For tests with sodium dodecylbenzene sulfonate (SDBS), 0.018 g of SDBS was added to 1 liter of 0.5 M NaOH solution. This was an arbitrary amount chosen after visually testing the mixing of different concentrations of SDBS in *toluene-water* solutions. The SDBS was added to the aqueous phase to avoid the risk of any reaction between the surfactant and the 4-NPA reactant before entering the reactor. The feed solution was kept mixed to ensure the SDBS concentration remained constant during the experiment.

Table 2.1. Physical Properties of Solvents at 23 ºC

Fluid	ρ [kg/m^3]	μ [$mPa \cdot s$]	Interfacial tension with water [mN/m]	Solubility in water [$mol\%$]
Toluene[19–21]	862	0.552	35.4	0.01
n-Butanol[19–21]	806	2.571	1.8	1.88
0.5 M NaOH in water [22]	1020	1.124	-	-

2.2.2. Test Reaction: Alkaline Hydrolysis of 4-Nitrophenyl Acetate

The two-phase alkaline hydrolysis of 4-nitrophenyl acetate (4-NPA, Scheme 1) was used to analytically measure the overall volumetric mass transfer coefficient of a given mixer. It has been shown that the kinetics have an intrinsic rate constant of 14.0 L/(mol s) for a second order reaction[23–25]. Using a 0.5 mol/L concentration of NaOH in water and 0.05 mol/L of 4-NPA in whichever organic solvent was being tested allowed for a 10:1 molar ratio of NaOH to 4-NPA (due to equal volumetric flow rates), causing pseudo-first order reaction conditions. In addition, the product, 4-nitrophenolate would turn the alkaline aqueous phase yellow when present, allowing for a visual distinction of the extent of reaction. Flow visualizations were taken using the reactor sight glass with a Nikon D40x "kit" camera fitted with an AF-S DX Zoom-Nikkor 18–55mm $f/3.5$–5.6 G ED II lens and the flow regimes were noted.

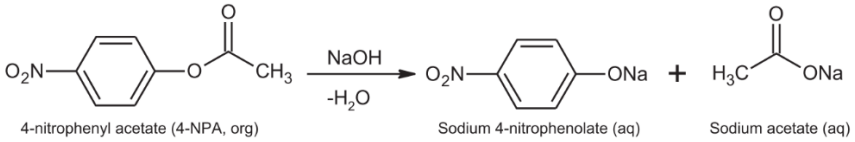

Scheme 1. Alkaline hydrolysis of 4-nitrophenyl acetate

A single experiment consisted of 7-9 flow rates being tested after flushing the system with reactants for 5 minutes at 10 mL/min. Once a new flow rate was set, the system was left at least three residence times to reach steady state before taking the sample. If three residence times lasts less than two minutes, two minutes was left between the change of flow rate and sampling to allow the operator sufficient time to prepare the next sample or take photographs of the flow regime if required. The sample time for a given flow rate was the larger of three residence times or 5 seconds. Samples were taken at the outlet into a quench solution; an agitated mixture of acetonitrile, water, and acetic acid that homogenized and neutralized the reactor effluent. The

quench solution composition was based on the particular solvent since different amounts of acetonitrile are required to homogenize the outlet sample. The samples were analyzed with an HP Agilent 1100 series HPLC system with a 250mm × 4.6mm i.d. Agilent Zorbax SB-C8 at room temperature.

2.3. Results and Discussion

All four geometries studied, and the specifications of their reactor plates can be found in Table 2.2. The micro-mixers were manufactured as exchangeable plates onto a FlowPlate® Lab (size A7, seen in Figure 2.3) reactor unit, which allows for visualization of the flow regimes through a glass viewport. Size 600 micro-mixers have a hydraulic diameter measured at the narrowest contraction, d_h, of 286 μm (width of 0.2 mm, depth of 0.5 mm). Scaled-up versions of the LL-Rhombus and LL-Triangle were also studied, and the specifications of these reactor plates can be found in Table 2.3. The size 300 mixers were designed with a d_h of 714 μm (width of 0.5 mm, depth of 1.25 mm); a diameter that allows for roughly a 10x scale-up of flow rate for constant energy dissipation[13]. An example of both reactor plate scales can be seen in Figure 2.4. Note that the term *reactor plate* refers to an entire reactor with multiple micro-mixers, while *mixer* or *mixing unit* relates to a particular mixing element.

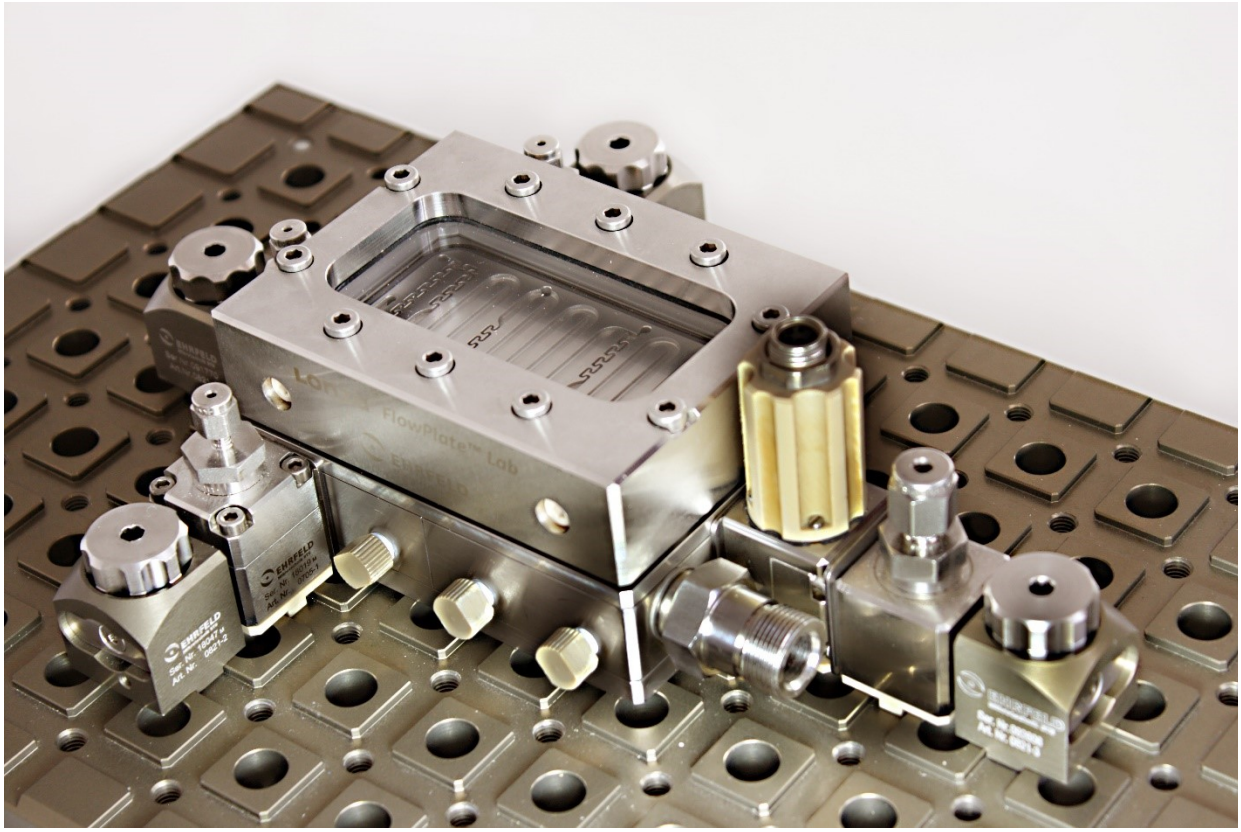

Figure 2.3. A FlowPlate® Lab reactor system setup

Table 2.2. Size 600 micro-mixer geometries studied and number of mixers per plate-reactor with a d_h of 286 μm (width of 0.2 mm, depth of 0.5 mm)

Structure	Repeating Element	N_{mixer}	Volume (mL)
Sickle		71	0.48
LL-Rhombus		88	0.24
LL-Triangle		88	0.24
LL-Empty		88	0.25
	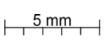		

Table 2.3. Size 300 micro-mixer geometries studied and number of mixers per plate-reactor with a d_h of 714 μm (width of 0.5 mm, depth of 1.25 mm)

Structure	Repeating Element	N_{mixer}	Volume (mL)
LL-Rhombus	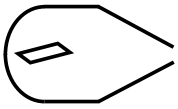	21	0.95
LL-Triangle	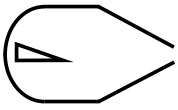	21	0.95

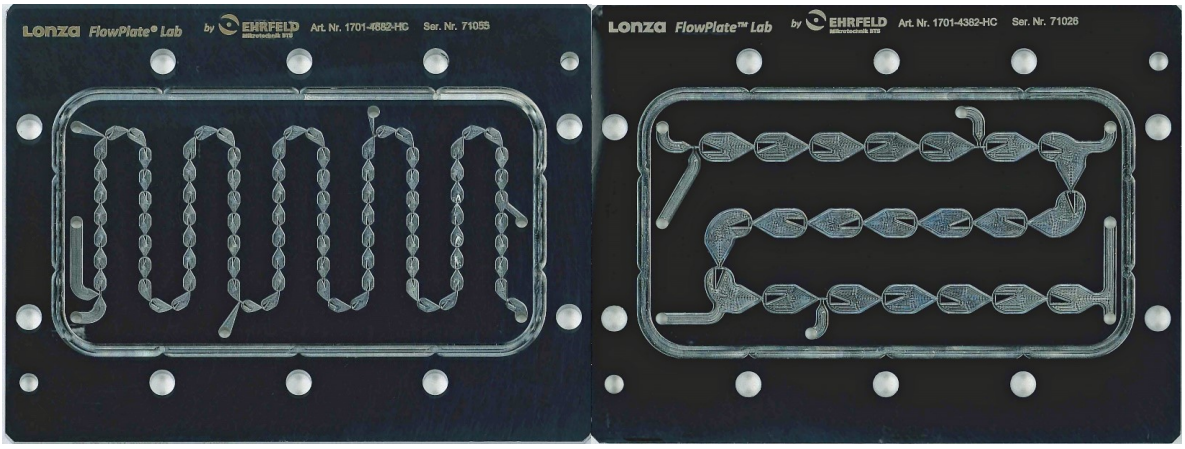

Figure 2.4. Examples of size 600 (left) and 300 (right) A7 reactor plates for the FlowPlate® Lab reactor system

The first study compares the different geometries at the smaller scale, size 600 both visually and analytically using the alkaline hydrolysis of 4-nitrophenyl acetate. The product of the reaction, sodium 4-nitrophenolate, colors the aqueous phase yellow and allows visual distinction between the two phases and qualitatively the extent of the reaction. *Toluene-water* and *n-butanol-water* systems were chosen as the initially tested solvent pairs due to their widely different physical properties as shown in Table 2.1. *Toluene-water* represents a high interfacial tension system with low solubility in water (0.01 mol %) whereas *n-butanol-water* has a much lower interfacial tension and greater solubility (1.88 mol %). Using these solvents allows for the evaluation of the geometries across a wide range of experimental conditions.

Since the LL-Triangle and LL-Rhombus geometries are similar, further comparison was performed with a *toluene-water* system with the presence of a surfactant, sodium dodecylbenzene sulfonate (SDBS). This was done in order to determine if the slug/drop flow regime could be eliminated in systems with interfacial tensions between that of *n-butanol-water* and *toluene-water*. Finally, to confirm the applicability of scale-up rules in micro-mixers[13], the LL-Triangle mixer was tested with *n-butanol-water* and *toluene-water* systems at the larger mixer size 300. In all of the studies, the main objective was to determine which micro-mixer could generate drop flow (and therefore highest $K_{org}a$) at the lowest average rate of energy dissipation for a given solvent system.

2.3.1. All Geometries Comparison

2.3.1.1. Visualization of Flow Regimes

In studying multi-phase mixing in micro-reactors, it is important first to investigate the flow regimes that occur[11,12,14]. Previous work distinguished between three distinct flow regimes: slug, parallel, and drop flow[12]. In the present study, combinations of these flow regimes were observed at different flow rates in each of the reactors studied. In addition, *dispersed* flow is defined to be a subset of drop flow where droplets are too small to be resolved visually and are seen as an emulsion. It is important to note that this is not a meaningful change in flow regime, but rather a qualitative point that can be observed visually. The flow regimes in the *n-butanol-water* systems for size 600 reactors are shown in Table 2.4 with the flow regime map in Figure 2.5.

Table 2.4. *n-butanol-water* flow regimes at various flow ranges (using interval notation) for the size 600 **(a)** Sickle; **(b)** LL-Rhombus; **(c)** LL-Triangle

Flow Regime $\left[\text{Flow Rate } \left(\frac{\text{mL}}{\text{min}}\right)\right]$	**Visualization**	**Flow Regime** $\left[\text{Flow Rate } \left(\frac{\text{mL}}{\text{min}}\right)\right]$	**Visualization**
	(a) Sickle		**(b) LL-Rhombus**
Parallel/Drop [1.0 – 4.0]		**Slug/Drop** [1.0 – 3.0]	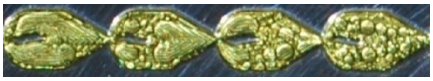
Parallel/Dispersed (4.0 – 7.0]	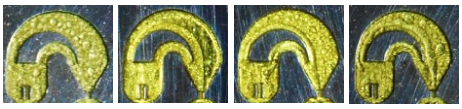	**Drop** (3.0 – 7.0]	
Dispersed (7.0 – 20.0]	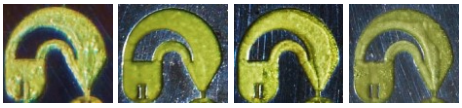	**Dispersed** (7.0 – 20.0]	
	(c) LL-Triangle		
Drop[a] [1.0 – 1.5]	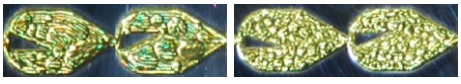		
Dispersed (1.5 – 20.0]	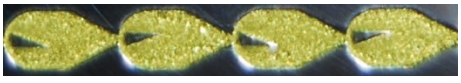		

[a] *Video of flow regime shown in Supplementary Material V.1.*

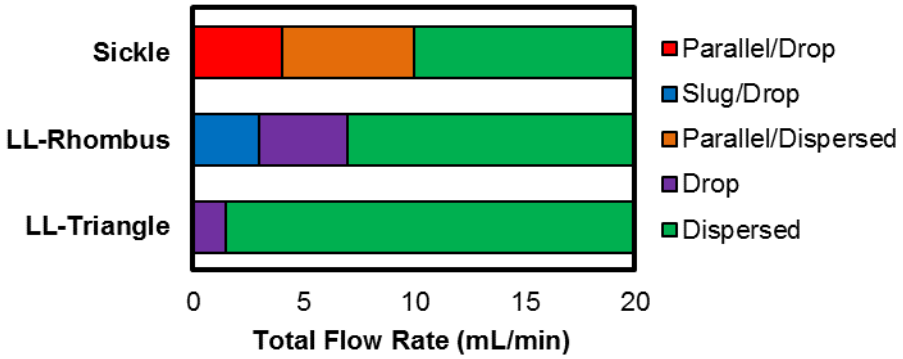

Figure 2.5. Flow regimes vs. flow rate for various size 600 geometries in an *n-butanol-water* system

In the Sickle reactor plate, parallel flow was observed in some form from 1.0 to 7.0 mL/min, while both LL mixers avoided this flow regime due to the minimization of curvature in the design. In fact, the LL-Triangle achieved drop flow at flow rates as low as 1.0 mL/min, whereas the LL-Rhombus required at least 3.0 mL/min.

Table 2.5 shows the flow regimes observed in the *toluene-water* system for all four geometries studied, and Figure 2.6 shows the flow regime map for the Sickle, LL-Rhombus, and LL-Triangle. The LL-empty was not included in the map as it is not an obstacle-based micro-mixer, and therefore has different flow regimes than the other mixers, as depicted in Table 2.5.

Table 2.5. *Toluene-water* flow regimes at various flow ranges (using interval notation) for the size 600 **(a)** Sickle; **(b)** LL-Rhombus; **(c)** LL-Triangle; **(d)** LL-Empty

Flow Regime $\left[\text{Flow Rate } \left(\frac{\text{mL}}{\text{min}}\right)\right]$	Visualization	Flow Regime $\left[\text{Flow Rate } \left(\frac{\text{mL}}{\text{min}}\right)\right]$	Visualization
	(a) Sickle		**(b) LL-Rhombus**
Slug [1.0 – 3.6]		**Slug** [1.0]	
Slug/Drop (3.6 – 8.0]		**Slug/Drop** (1.0 – 10.0]	
Drop (8.0 – 20.0]		**Dispersed** (10.0 – 20.0]	
	(c) LL-Triangle		**(d) LL-Empty**
Slug/Drop[b] [1.0 – 10.0]		**Slug** [1.0]	
Dispersed[b] (10.0 – 20.0]		**Slug/Jet/Drop** (1.0 – 5.0]	
		Jet/Drop (5.0 – 20.0]	

[b] Video of flow regime shown in Supplementary Material V.2.

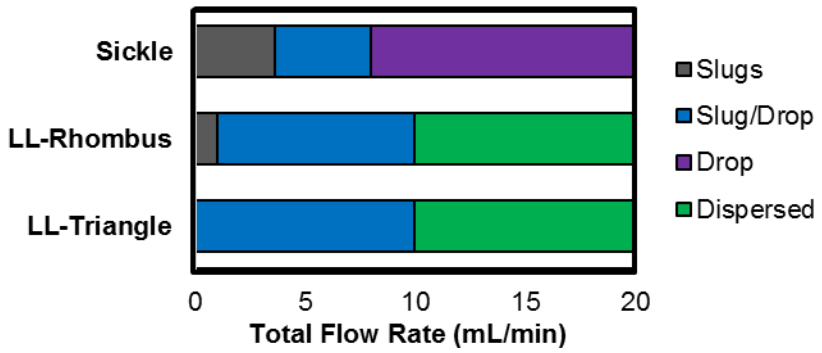

Figure 2.6. Flow regimes vs. flow rate for various size 600 geometries in a *toluene-water* system

As the *toluene-water* system has a greater interfacial tension than *n-butanol-water*, it is expected that higher flow rates are required for the onset of drop flow. In addition, parallel flow was not

likely to be observed in any micro-mixers with this solvent system[12]. When comparing the Sickle to the two LL mixers with obstacles, the Sickle required higher flow rates to begin the break-up of slugs. While the onset of drop flow in the Sickle mixer occurs at 8 mL/min, the LL-Rhombus and LL-Triangle were already in a slug/drop regime as early as 1.5 and 1.0 mL/min, respectively. This unstable transition regime has a significant improvement over the slug flow regime that is present in the Sickle in terms of the overall volumetric mass transfer coefficient, as will be discussed further. The visualization of the flow regimes in the LL-Empty (Table 2.5d) show that an obstacle is required to avoid jetting through the reactor.

2.3.1.2. Analytical Results from the Alkaline Hydrolysis of 4-NPA

In addition to studying the flow regimes visually, $K_{org}a$ can be measured analytically through the test reaction of 4-NPA[11–13] with NaOH due to the fast kinetics of the reaction[23–25], and the insolubility of 4-NPA in the aqueous NaOH solution (less than 2.5 mmol/L at 23 °C). First, the different geometries are evaluated based on the conversion vs. total flow rate (Q_{tot}). These results are presented in Figure 2.7 for *n-butanol-water* (a) and *toluene-water* (b).

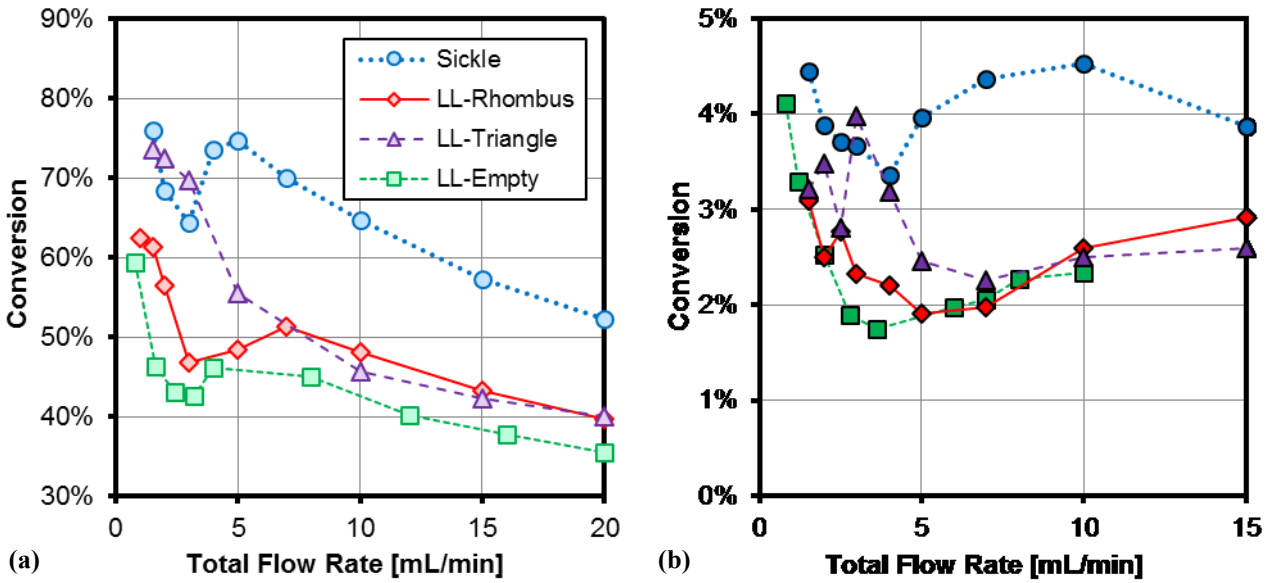

Figure 2.7. Conversion vs. total volumetric flow rate for **(a)** *n-butanol-water* (light) and **(b)** *toluene-water* (dark) systems with different size 600 micro-mixer geometries using the alkaline hydrolysis of 4-NPA

Most of the results follow a similar trend when increasing the flow rate. There is an initial decrease in conversion for the first flow rates below 3 mL/min, followed by a slight rise in conversion with flow. For *n-butanol-water*, the final increase reaches a plateau and begins to decrease with flow, whereas the conversion steadily increases with flow for the *toluene-water* system.

When studying these conversion data, note that there are competing factors when increasing the flow rate while in a given flow regime. Residence time decreases with flow, but the mass transfer rate increases with more energy being dissipated into the system through pressure loss. In a given flow regime, such as slug or parallel flow, the reduction in residence time is generally a greater factor, as indicated by the negative slopes in these regions. However, transitions between flow regimes can lead to a significant variation in interphase mass transfer rate, therefore causing a pronounced change in conversion. This occurs in the transition to drop flow, where the specific area available for mass transfer increases substantially. For the *toluene-water* system in the drop flow regime, increasing flow can actually have an increase in conversion due to the reduction in droplet size outcompeting the reduction in residence time for flow rates above 5 mL/min.

In the *toluene-water* system, the LL-Triangle and LL-Rhombus perform similarly, with the exception of the slug/drop flow regime; which will be discussed further when directly comparing the two LL obstacles in section 2.2. For both solvent systems, the obstacles in the LL-Triangle and LL-Rhombus increased the conversion when compared with the LL-Empty as expected, since jetting was visible in Table 2.5d. This would create stagnant zones; reducing the surface area available for mass transfer.

It is important to recognize that the reacting volume in the Sickle plate is roughly double that of the three LL plates, causing the conversion for the Sickle to be significantly greater. However, the LL-Triangle results are particularly interesting, as the flow visualizations show that it achieves drop flow in *n-butanol-water* at the lowest flow rate (as seen in Table 2.4c and Figure 2.5). The benefit can clearly be seen in Figure 2.7a where the LL-Triangle, with half the residence time, has conversions in the range of the Sickle at low flows. The LL-Triangle also does not show any increase in conversion with flow rate because it has already reached the desired drop flow regime.

While the conversion vs. flow data is interesting in interpreting the flow regime results, it is more useful to look at the $K_{org}a$ vs. ε since these terms normalize for reactor volume and pressure loss across the length of the reactor, allowing for the direct comparison between different micro-mixers. The measured conversion can be related to the overall volumetric mass transfer coefficient with equation (2.1) by assuming: interphase mass transfer rate is fully rate-limiting; the two phases are both considered in plug flow; no-slip velocity of the phases.

$$K_{org}a = -\frac{\varphi_{org}}{\tau}\ln(1-\eta) \tag{2.1}$$

The average rate of energy dissipation is defined in equation (2.2) and represents the total flow rate normalized by the reactor volume and total pressure drop. It is based on the density of the continuous phase, which is the aqueous phase due to the wetted material being stainless steel or Hastelloy C22™.

$$\varepsilon = \frac{\Delta P Q_{tot}}{\rho_c V_R} = \frac{\Delta P}{\rho_c \tau} \tag{2.2}$$

Comparing $K_{org}a$ vs. ε allows for the analysis of different reactor geometries, regardless of total reactor volume or number of mixers, and highlights the most efficient geometry for generating a fine dispersion while using the least energy. The results for all four geometries with *n-butanol-water* and *toluene-water* can be seen in Figure 2.8.

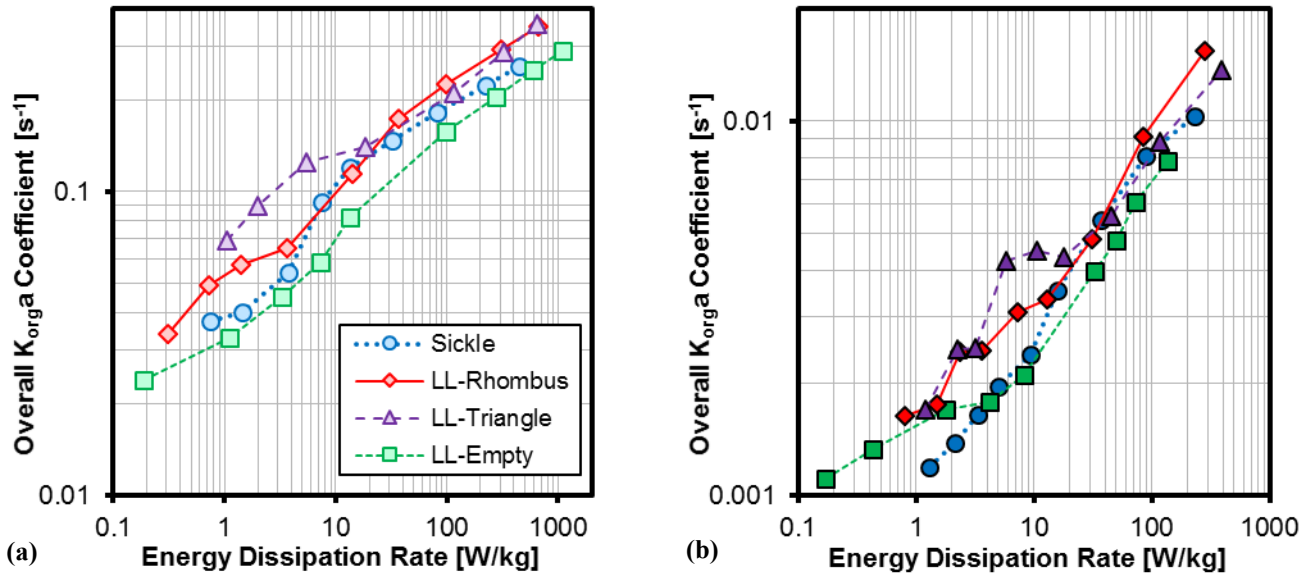

Figure 2.8. Overall volumetric mass transfer coefficient vs. the average rate of energy dissipation for **(a)** *n-butanol-water* (light) and **(b)** *toluene-water* (dark) systems with different size 600 micro-mixer geometries using the alkaline hydrolysis of 4-NPA

It is clear that both of the LL mixers with obstacles achieve higher $K_{org}a$ than the Sickle and LL-Empty mixers at low flow rates. In addition, the LL-Triangle benefits significantly in the *n-butanol-water* system due to the onset of the drop flow regime at low energy dissipations. In the *toluene-water* system, the slug/drop flow regime shows the only difference between the LL-

Triangle and LL-Rhombus. Both mixers outperform the Sickle and LL-Empty in the low flow ranges and, once all mixers have reached drop flow, the $K_{org}a$ vs. ε converge, as expected[11].

While the LL-Empty results seem to be an exception for the convergence of $K_{org}a$ vs. ε in drop flow, a possible explanation for the results to be consistently lower than the other plates could be due to dead zones from bypassing. This reactor volume is included in the calculation of $K_{org}a$ and ε, but no significant reaction is occurring. This further shows that the obstacles in the LL plates allow the geometry to better utilize the reacting volume.

It is interesting to note that the results in the slug/drop flow regime are not consistent between repeated runs with the toluene-water. Figure 2.9 shows four repeated runs with the LL-Rhombus and two with the LL-Triangle. It can be seen that the point at which the flow regime transitions from slug to drop flow is not a set energy dissipation, but a range between 2 and 10 W/kg. This can be considered analogous to the single-phase transition from laminar to turbulent flow where, at a given Reynolds number between 2300 and 4000, either laminar or turbulent flow is observed[26]. The actual flow regime is subject to environmental factors such as the uniformity of the fluid's velocity or the wall roughness. It is possible that in a two-phase system during the transition from slug to drop flow, the system was particularly sensitive to uncontrollable factors such as syringe changeover in the pumps (causing slight interruptions in flow every 5-30 seconds).

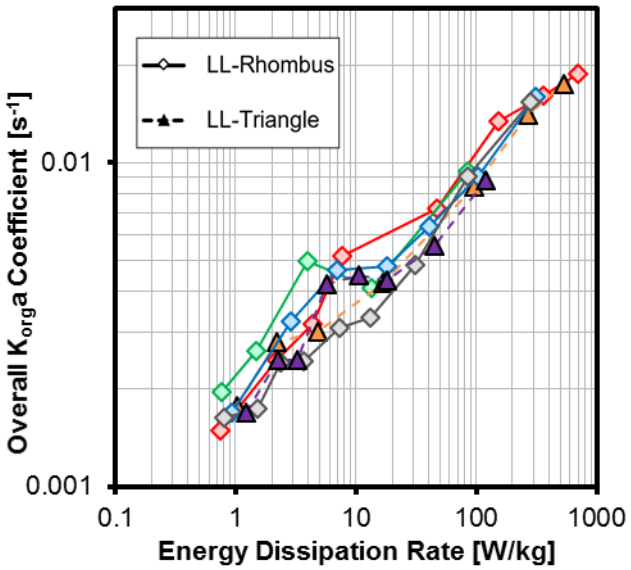

Figure 2.9. Six repeated experiments for the overall volumetric mass transfer coefficient vs. the average rate of energy dissipation for *toluene-water* with the size 600 LL-Rhombus and LL-Triangle using the alkaline hydrolysis of 4-NPA

While stochastic variations from experiment to experiment were observed, the specific flow regime for a given test is established once the flow rates from the pump achieve steady-state (i.e. no lag-time at start-up). For this reason, multiple samples were not performed at a given flow rate, but instead averaged over three to ten residence times. The "development" of the flow regimes, if any, occurs in the first one to five mixing units (one for highest flow rates, five for lower flow rates as seen in V.3. in the supporting information).

2.3.2. Further Comparison of LL Mixers

2.3.2.1. Visualization of Flow Regimes for the Toluene-water with SDBS System

The comparison of the LL-Triangle and LL-Rhombus was continued because of their strong performance relative to the Sickle. To accomplish this, tests were performed with a *toluene-water* system with the addition of the surfactant SDBS. Since droplets were formed for all flow rates in the *n-butanol-water* system, but not *toluene-water*, it is important to know the flow regimes for systems with interfacial tensions between those solvent-pairs. The *toluene-water with SDBS* was investigated to determine if the slug/drop flow regime could be avoided to allow for an earlier onset of drop flow. Table 2.6 and Figure 2.10 show the observed flow regimes and flow regime map, respectively, for the LL-Rhombus and LL-Triangle reactors. Indeed, the addition of

surfactant significantly reduces the flow rate required for the onset of drop flow, with no tested flow rates exhibiting slug flow.

Table 2.6. Flow regimes at various flow ranges (using interval notation) for the size 600 LL-Rhombus **(a)** and LL-Triangle **(b)** with *toluene-water with SDBS* surfactant

Flow Regime $\left[\text{Flow Rate } \left(\frac{\text{mL}}{\text{min}}\right)\right]$	**(a) LL-Rhombus Visualization**	**Flow Regime** $\left[\text{Flow Rate } \left(\frac{\text{mL}}{\text{min}}\right)\right]$	**(b) LL-Triangle Visualization**
Drop [1.0 – 3.0]		**Drop** [1.0 – 2.0]	
Dispersed (3.0 – 15.0]		**Dispersed** (2.0 – 15.0]	

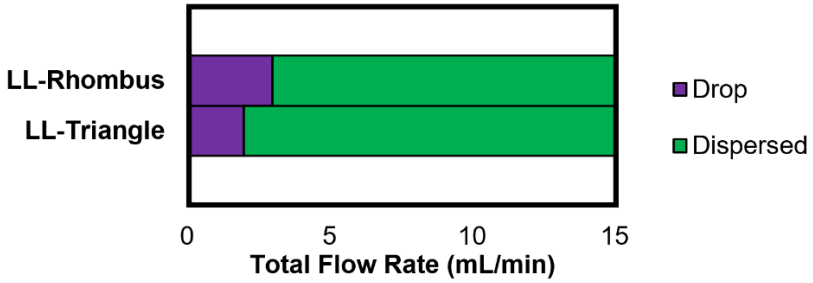

Figure 2.10. Flow regimes vs. flow rate for the size 600 LL-Rhombus and LL-Triangle in a *toluene-water with SDBS* system

2.3.2.2. Analytical Results from the Alkaline Hydrolysis of 4-NPA with the Toluene-water with SDBS System

The *toluene-water with SDBS* results for conversion vs. volumetric flow rate are presented in Figure 2.11. These analytical results follow expected trends since Table 2.6 shows that the flow regimes in both LL mixers were drop or dispersed for all flow rates tested. Since both plates have the same total volume and are in the same flow regimes for both solvent systems, it follows that the conversions should be similar as well.

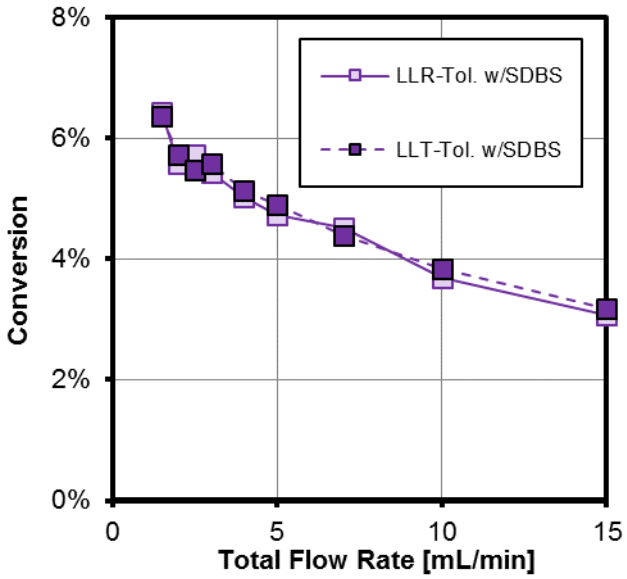

Figure 2.11. Conversion vs. total volumetric flow rate for *toluene-water with SDBS* systems for the size 600 LL-Rhombus (LLR, light, solid line) and the LL-Triangle (LLT, dark, dashed line) using the alkaline hydrolysis of 4-NPA

It is worth considering all three solvent systems together for the LL-Rhombus and LL-Triangle for the $K_{org}a$ vs. ε. Figure 2.12 shows evidently that the two mixer geometries perform similarly in the drop flow regime, but the LL-Triangle can reach that flow regime at lower flow rates/energy dissipations. The reason for this is most likely due to the flow's impingement against the base of the triangle obstacle, whereas the LL-Rhombus' obstacle uses a slicing mechanism of mixing. Looking at the visualizations for the lowest flows in Table 2.5 (b) and (c), it can be seen that the LL-Rhombus allows slugs to pass a single side of the obstacle while the LL-Triangle forces the slug to be split around it. Note that if the obstacle forced a complete change in flow direction (e.g. a curved obstacle), this could potentially cause parallel flow due to differences in solvent densities[11].

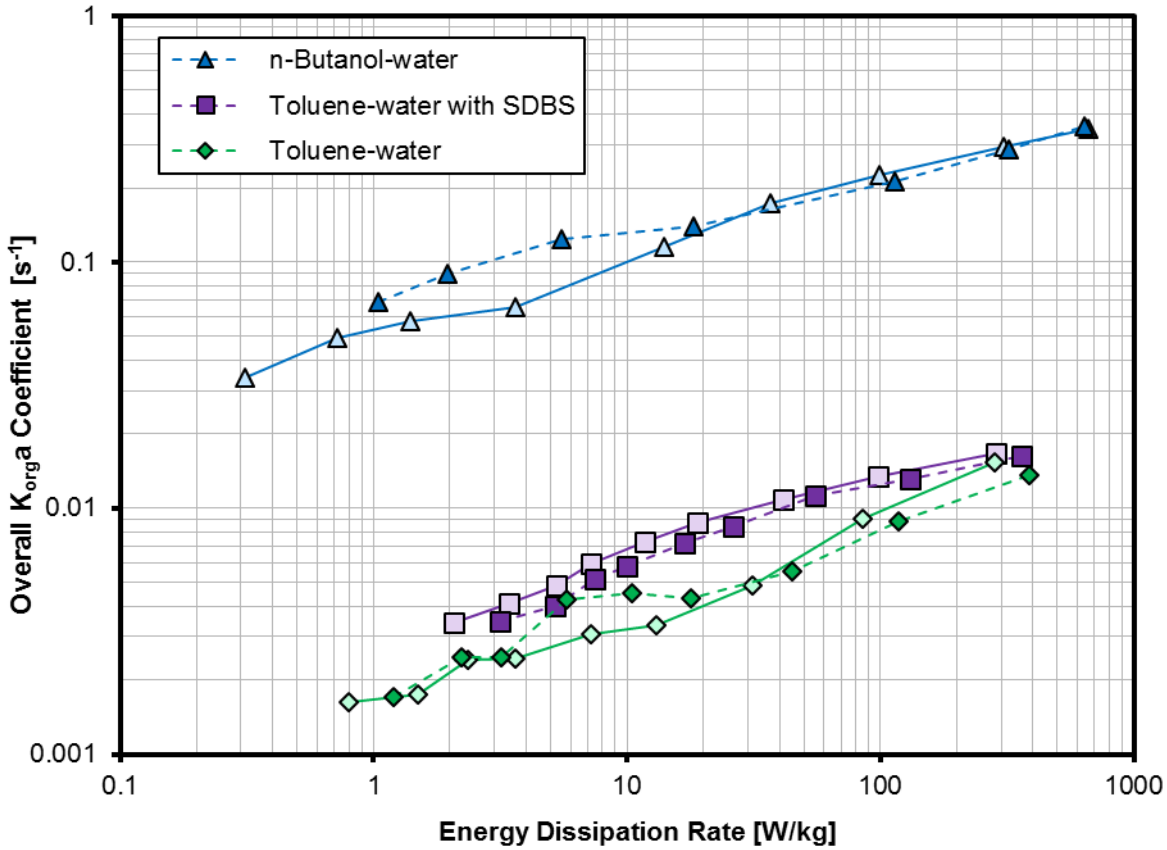

Figure 2.12. Overall volumetric mass transfer coefficient vs. the average rate of energy dissipation with various solvents for the size 600 LL-Rhombus (light, solid line) and the LL-Triangle (dark, dashed line) using the alkaline hydrolysis of 4-NPA

While it is interesting that the analytical results of $K_{org}a$ for the *toluene-water with SDBS* system eventually converge with the system without surfactant, it is not possible to say that the droplet sizes would be equal at the highest energy dissipation. There are several factors affecting the rate of interphase mass transfer when surfactant is present. For example, the surfactant can reduce the droplet size; however, this can be counteracted by a reduction in the mass transfer coefficient across the film (K_{org}) due to the known surface-immobilization of the interface in liquid-liquid[27] and gas-liquid[28–30] systems. The key finding from testing with the surfactant was the ability to eliminate the unstable slug/drop flow regime observed in the *toluene-water* system and obtain consistent and repeatable mass transfer coefficients.

2.3.3. Scale-up of LL Plates

2.3.3.1. Visualization of Flow Regimes

Previous work[13] studied the scale-up of the LL-Rhombus using the "3/7th" scaling rule to maintain constant rates of energy dissipation at flow rates roughly 10 times those in the size 600. This led to mixers designed with a hydraulic diameter of 714 μm in the size 300 mixers. Plouffe et al. showed that the scale-up of the LL-Rhombus achieved similar overall volumetric mass transfer coefficients for constant energy dissipations at both scales when in the drop flow regime. This was because the continuous phase is likely turbulent in the drop flow regime where chaotic eddies dissipate their energy partly via the creation of interfacial area, which leads to smaller drop sizes that are no longer function of the channel diameter such as for slugs. In order to confirm the application of the scale-up rule, a size 300 LL-Triangle plate was manufactured and tested with *n-butanol-water* and *toluene-water* systems for flow rates from 10 to 150 mL/min. Figure 2.13 shows the flow regime map for the various solvents; directly comparing the LL-Rhombus and LL-Triangle for the scaled-up mixers. The observed flow regimes follow a similar trend to what was seen in the size 600 mixers (with $Q_{300} \cong 10 \times Q_{600}$). Again, the LL-Triangle achieved the drop flow regime at the lowest flow rate studied in *n-butanol-water*, while the flow regimes were quite similar between the two mixers for the *toluene-water* system.

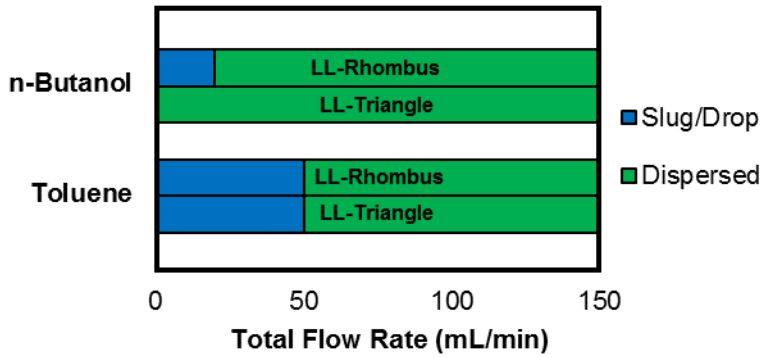

Figure 2.13. Flow regimes vs. flow rate for the size 300 LL-Rhombus and LL-Triangle in n-butanol-water, and toluene-water systems (lowest flow rate was 10 mL/min)

2.3.3.2. Analytical Results from the Alkaline Hydrolysis of 4-NPA

While the analytical results for the scale-up of the LL-Rhombus are presented in previous work[13], it is important to confirm the results for the novel LL-Triangle. Figure 2.14 shows the $K_{org}a$ vs. ε for both sizes 600 and 300 in *n-butanol-water* and *toluene-water* systems; the two systems with the widest range of interfacial tensions. While there are some differences between

the two scales, particularly at low flow rates, the plates generally follow the same trend, and, in the drop flow regime, converge to similar values as expected when applying the "3/7th" scaling rule.

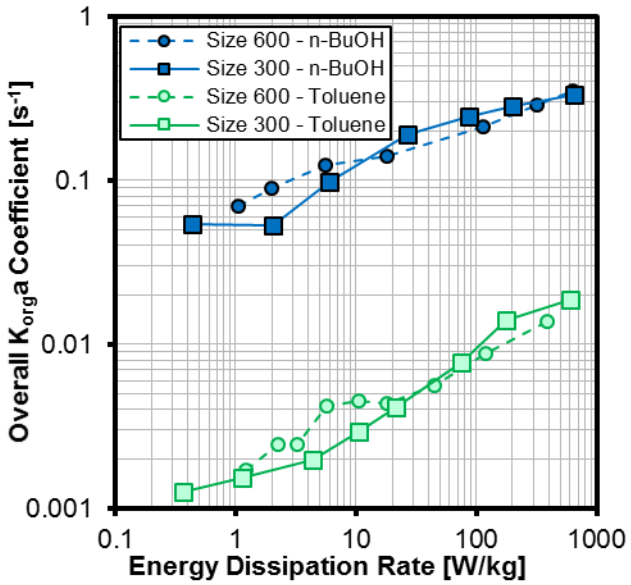

Figure 2.14. Overall volumetric mass transfer coefficient vs. average rate of energy dissipation for *n-butanol-water* (dark blue) and *toluene-water* (light green) systems with the size 600 (○) and 300 (□) LL-Triangle mixer using the alkaline hydrolysis of 4-NPA

Additionally, when comparing the $K_{org}a$ vs. ε for the LL-Rhombus and LL-Triangle in the size 300 mixers, similar trends are observed as in the size 600. Figure 2.15 shows that the LL-Triangle is still more effective than the LL-Rhombus at low flows, but otherwise, they are quite similar. Not only does this further prove the applicability "3/7th" scale-up rule for LL-mixers, but it shows that the LL-Triangle is an effective tool for the process development of new mass-transfer-limited reactions to larger scales.

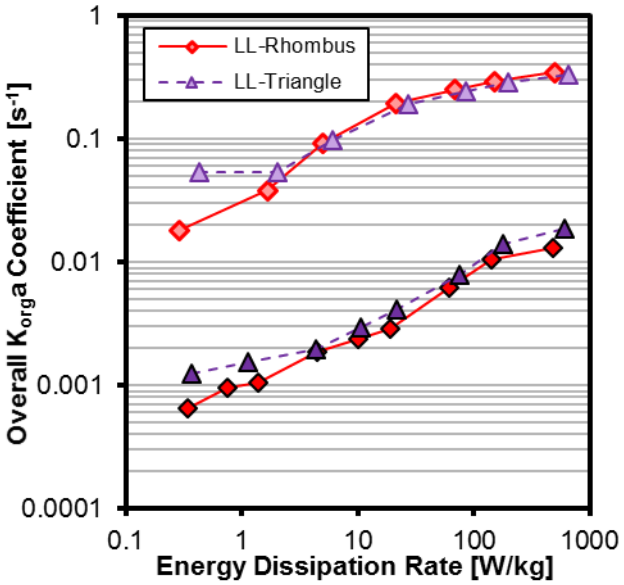

Figure 2.15. Overall volumetric mass transfer coefficient vs. the average rate of energy dissipation for *n-butanol-water* (light) and **(b)** *toluene-water* (dark) systems with the size 300 LL-Rhombus and LL-Triangle using the alkaline hydrolysis of 4-NPA

It is important to note that size 300 mixers are intended to be used on a larger micro-reactor system than the FlowPlate® Lab (size A7) and they were manufactured primarily for flow-visualization purposes. The scaled-up reactor plates can only fit 21 mixing units whereas, for example, the FlowPlate A6 system could fit 113 mixers. There is presumably a minimum number of mixers required to reach a given fully developed flow regime and this entrance region in the size 300 A7 plate is likely significant when comparing with results from size 600 plates.

Additionally, the FlowPlate Lab (size A7) system inlet and outlet ports are on the same order of magnitude in hydraulic diameter as the size 300 mixers, and with the higher flows being studied, it is no longer applicable to assume that the energy dissipation, and therefore the mixing, in the outlet is negligible.

2.4. Conclusions

Several obstacle-based micro-mixer geometries were studied with up to four different solvent-pair systems for two different mixer sizes. The liquid-liquid systems were observed and classified based on some combination of the following flow regimes: slug flow; parallel flow; or drop flow. For applications in fast liquid-liquid reactions, drop flow is the ideal flow regime due to the increased specific area available for interphase mass transfer. The alkaline hydrolysis of 4-nitrophenyl acetate was used as a test reaction to measure analytically the overall volumetric mass

transfer coefficients in the various mixers. The micro-mixers were evaluated based on the $K_{org}a$ plotted vs. the average rate of energy dissipation to determine the most efficient mixer design (i.e., the mixer with the earliest onset of drop flow).

In the flow range of 1-20 mL/min, the novel LL-Triangle micro-mixer design was shown to perform equally well as or better than any of the other micro-mixers studied in all solvent-pairs investigated, namely the Sickle, the LL-Rhombus, and the LL-Empty. The benefits for this mixer were most clearly observed at low flow rates for low interfacial tension systems, such as *n-butanol-water*, where the drop flow regime was observed at the lowest energy dissipation. In the *toluene-water* system, both LL-mixers performed similarly, with a slug/drop flow regime observed for low flows. It was possible to avoid this transition regime with the use of a surfactant in the *toluene-water* system. Drop flow was observed in both LL-mixers at lower energy dissipations than the Sickle mixer and unwanted parallel flow was avoided due to the reduced curvature.

The results were reproduced in a larger scale LL-Triangle for flow rates between 10-150 mL/min where the LL-Triangle achieved drop flow again for all flow rates studied in *n-butanol-water*. The overall volumetric mass transfer coefficients were similar to those obtained at equal energy dissipations in the smaller scale in the drop flow regime; indicating that the LL-Triangle micro-mixer is excellent for the process development and scale-up of fast liquid-liquid reactions. Finally, for liquid-liquid reactive systems, this work nicely shows that a flow visualization is of prime importance to enable determination of the proper flow regime and ensure consistent scale-up.

2.5. Nomenclature

Symbol	Description (units)
General	
a	specific interfacial area of contact (m^2/m^3)
b	width of the channel at contraction (m)
d_h	hydraulic diameter at contraction $= \boldsymbol{2hb/(h+b)}$ (m)
h	depth of the channel at contraction (m)
K	overall convective mass transfer coefficient (m/s)
Q	volumetric flow rate (m^3/s)
V	Volume (m^3)
ΔP	Pressure drop across the reactor (Pa)
Greek Symbols	
ε	average rate of energy dissipation (W/kg)
η	conversion (%)

μ	fluid viscosity (Pa·s)
ρ	fluid density (kg/m^3)
σ	fluid interfacial tension with water (N/m)
τ	average residence time (s)
φ	volumetric phase fraction

Subscripts

aq	aqueous phase
c	continuous phase
d	dispersed phase
org	organic phase
tot	total (sum of organic and aqueous phase)
R	reactor
300	in a size 300 micro-mixer; d_h = 714 μm
600	in a size 600 micro-mixer; d_h = 286 μm

Acknowledgements. The authors would like to thank the Natural Sciences and Engineering Research Council of Canada, including the CREATE program in Continuous Flow Science, and Lonza AG for their financial contribution. Also, Ehrfeld Mikrotechnik BTS is acknowledged for the reactor manufacturing.

Supporting Information Available: Supplementary videos of various flow regimes (*V.1., LL-Triangle — n-Butanol-water.mp4; V.2., LL-Triangle —Toluene-water.mp4; V.3., LL-Triangle Size 300 — n-Butanolwater.mp4*) associated with this article can be found in the online version at doi: 10.1556/1846.2016.00026.

2.6. References

[1] V. Kumar, M. Paraschivoiu, K.D.P. Nigam, Single-phase fluid flow and mixing in microchannels, Chem. Eng. Sci. 66 (2011) 1329–1373. doi:10.1016/j.ces.2010.08.016.

[2] C.P. Holvey, D.M. Roberge, M. Gottsponer, N. Kockmann, A. Macchi, Pressure drop and mixing in single phase microreactors: Simplified designs of micromixers, Chem. Eng. Process. Process Intensif. 50 (2011) 1069–1075. doi:10.1016/j.cep.2011.05.016.

[3] P. Plouffe, R. Anthony, A. Donaldson, D.M. Roberge, N. Kockmann, A. Macchi, Transport Phenomena in Two-Phase Liquid-Liquid Micro-Reactors, in: ASME 2012 10th Int. Conf. Nanochannels, Microchannels, Minichannels, Rio Grande, Puerto Rico, 2012. http://proceedings.asmedigitalcollection.asme.org/proceeding.aspx?articleid=1719073 (accessed August 19, 2014).

[4] N. Kockmann, M. Gottsponer, D.M. Roberge, Scale-up concept of single-channel microreactors from process development to industrial production, Chem. Eng. J. 167 (2011) 718–726. doi:10.1016/j.cej.2010.08.089.

[5] M. Kashid, A. Renken, L. Kiwi-Minsker, Mixing efficiency and energy consumption for five generic microchannel designs, Chem. Eng. J. 167 (2011) 436–443. doi:10.1016/j.cej.2010.09.078.

[6] L. Falk, J.M. Commenge, Performance comparison of micromixers, Chem. Eng. Sci. 65 (2010) 405–411. doi:10.1016/j.ces.2009.05.045.

[7] V. Hessel, D. Kralisch, N. Kockmann, T. Noel, Q. Wang, Novel Process Windows for Enabling, Accelerating, and Uplifting Flow Chemistry, ChemSusChem. 6 (2013) 746–789. doi:10.1002/cssc.201200766.

[8] L. Ducry, D.M. Roberge, Controlled Autocatalytic Nitration of Phenol in a Microreactor, Angew. Chemie - Int. Ed. 44 (2005) 7972–7975. doi:10.1002/anie.200502387.

[9] M.N. Kashid, L. Kiwi-Minsker, Microstructured Reactors for Multiphase Reactions: State of the art, Ind. Eng. Chem. Res. 48 (2009) 6465–6485. doi:10.1021/ie8017912.

[10] G. Dummann, U. Quittmann, L. Gröschel, D.W. Agar, O. Wörz, K. Morgenschweis, The Capillary-Microreactor: A New Reactor Concept for the Intensification of Heat and Mass Transfer in Liquid-Liquid Reactions, Catal. Today. 79–80 (2003) 433–439. doi:10.1016/S0920-5861(03)00056-7.

[11] P. Plouffe, D.M. Roberge, A. Macchi, Liquid–liquid flow regimes and mass transfer in various micro-reactors, Chem. Eng. J. 300 (2016) 9–19. doi:10.1016/j.cej.2016.04.072.

[12] P. Plouffe, D.M. Roberge, J. Sieber, M. Bittel, A. Macchi, Liquid–liquid mass transfer in a serpentine micro-reactor using various solvents, Chem. Eng. J. 285 (2016) 605–615. doi:10.1016/j.cej.2015.09.115.

[13] P. Plouffe, M. Bittel, J. Sieber, D.M. Roberge, A. Macchi, On the scale-up of micro-reactors for liquid–liquid reactions, Chem. Eng. Sci. 143 (2016) 216–225. doi:10.1016/j.ces.2015.12.009.

[14] P. Plouffe, A. Macchi, D.M. Roberge, From batch to continuous chemical synthesis-a toolbox approach, Org. Process Res. Dev. 18 (2014) 1286–1294. doi:10.1021/op5001918.

[15] M.J. Nieves-Remacha, A. a. Kulkarni, K.F. Jensen, Gas–Liquid Flow and Mass Transfer in an Advanced-Flow Reactor, Ind. Eng. Chem. Res. 52 (2013) 8996–9010. http://dx.doi.org/10.1021/ie4011707.

[16] E.D. Lavric, P. Woehl, Advanced-Flow TM glass reactors for seamless scale-up, Chem. Today. 27 (2009) 45–48.

[17] M. N. Kashid, A. Renken, L. Kiwi-Minsker, Influence of Flow Regime on Mass Transfer in Different Types of Microchannels, Ind. Eng. Chem. Res. 50 (2011) 6906–6914. doi:10.1021/ie102200j.

[18] M.J. Nieves-Remacha, A.A. Kulkarni, K.F. Jensen, Hydrodynamics of Liquid–Liquid Dispersion in an Advanced-Flow Reactor, Ind. Eng. Chem. Res. 51 (2012) 16251–16262. doi:10.1021/ie301821k.

[19] H.M. Backes, J.J. Ma, E. Bender, G. Maurer, Interfacial tensions in binary and ternary liquid—liquid systems, Chem. Eng. Sci. 45 (1990) 275–286. doi:10.1016/0009-2509(90)87099-E.

[20] A. Berthod, N. Schmitt, Water—organic solvent systems in countercurrent chromatography: Liquid stationary phase retention and solvent polarity, Talanta. 40 (1993) 1489–1498. doi:10.1016/0039-9140(93)80358-X.

[21] D.J. Donahue, F.E. Bartell, The Boundary Tension at Water-Organic Liquid Interfaces, J. Phys. Chem. 56 (1952) 480–484. doi:10.1021/j150496a016.

[22] A.A. Alexandrov, The Equations for Thermophysical Properties of Aqueous Solutions of Sodium Hydroxide, 14th Int. Conf. Prop. Water Steam. (2005) 86–90. http://www.iapws.jp/Proceedings/Symposium02/086Alexandrov.pdf.

[23] B. Ahmed-Omer, D. Barrow, T. Wirth, Effect of segmented fluid flow, sonication and phase transfer catalysis on biphasic reactions in capillary microreactors, Chem. Eng. J. 135 (2008) S280–S283. doi:10.1016/j.cej.2007.07.017.

[24] B. Ahmed, D. Barrow, T. Wirth, Enhancement of reaction rates by segmented fluid flow in capillary scale reactors, Adv. Synth. Catal. 348 (2006) 1043–1048. doi:10.1002/adsc.200505480.

[25] V.D. Parker, Instantaneous rate constants in physical organic chemistry: Application to acyl transfer reactions of p-nitrophenyl acetate to hydroxide ion, J. Phys. Org. Chem. 19 (2006) 714–724. doi:10.1002/poc.1064.

[26] M.C. Potter, D.C. Wiggert, B.H. Ramadan, Mechanics of Fluids, 4th ed., Cengage Learning, Stamford, CT, 2011.

[27] R. Clift, J.R. Grace, M.E. Weber, Bubbles, drops, and particles, Dover Publications, Inc., Mineola, New York, 1978.

[28] K. Koide, S. Yamazoe, S. Harada, Effects of Surface-Active Substances on Gas Holdup and Gas-Liquid Mass Transfer in Bubble Column., J. Chem. Eng. Japan. 18 (1985) 287–292.

[29] J.J. Jeng, J.R. Maa, Y.M. Yang, Surface effects and mass transfer in bubble column, Ind. Eng. Chem. Process Des. Dev. 25 (1986) 974–978. doi:10.1021/i200035a023.

[30] W.W. Eckenfelder, E.L. Barnhart, The effect of organic substances on the transfer of oxygen from air bubbles in water, AIChE J. 7 (1961) 631–634. doi:10.1002/aic.690070420.

3. Investigation of Overall and Localized Heat Transfer in Curved Micro-Channel Reactor Systems

Eric Mielke,[a] Patrick Plouffe,[a] Nikhil Koushik,[a] Markus Eyholzer,[b] Michael Gottsponer,[b] Norbert Kockmann,[c] Arturo Macchi[a,*] and Dominique M. Roberge,[b,*]

a, Centre for Catalysis Research and Innovation, Department of Chemical and Biological Engineering, University of Ottawa, K1N 6N5 Ottawa, Canada.

b, Chemical Manufacturing Technologies, Lonza AG, CH-3930 Visp, Switzerland.

c, University of Technology Dortmund, Biochemical and Chemical Engineering, Equipment Design, Emil-Figge-Str. 68, D-44227 Dortmund, Germany

This manuscript will be submitted for publication in 2017

ABSTRACT

Non-reactive and reactive heat transfer experiments were performed in the FlowPlate® system by Ehrfeld Mikrotechnik BTS, which is composed of alternating reactor and heat transfer fluid plates within a rack. The non-reactive system studied a rectangular serpentine channel with Reynolds numbers ranging from 400-2000, and a Gnielinski-type model was fit to the internal Nusselt number. A silver-based thermal paste was shown to reduce the external resistance to heat transfer between the reactor and heat transfer fluid plates by ~70%, leading to overall heat transfer coefficients of $\sim 2200\,[W/(m^2\,K)]$. In the reactive system, the synthesis of methyl 2-oxobutanoate, using dimethyl-oxalate and the Grignard reagent ethylmagnesium chloride, was highlighted as a test reaction to differentiate localized heat transfer characteristics across different reactors. The Grignard reaction was used to compare the impact of various micro-mixer geometries, materials, injection ports, and scales on hotspot formation in the reactors. Finally, an analysis of four case studies was presented using the fourth Damköhler number to determine a maximum channel diameter that would remove sufficient heat to avoid hotspot formation, based on experimentally determined overall heat transfer coefficients.

Keywords: Micro-reactor, overall heat transfer, localized heat transfer, transitional flow, serpentine channels

3.1. Introduction

The field of continuous-flow micro-reactor technology has been gaining academic and industrial interest in recent years due to its many advantages over batch processes at smaller scales [1–4]. Micro-reactors potentially offer enhanced transport rates including wall-to-fluid heat transfer due to relatively small channel dimensions and high surface-area-to-volume ratios when compared to batch or larger-scale continuous flow reactors [1–7]. Notwithstanding the fact that a single micro-reactor is not a general solution to all type of reactions [8], Plouffe et al. developed a toolbox approach where the preferred reactor system is chosen for the given reaction rate, reaction network, and phase type [9]. This toolbox encompasses the use of micro-structure plates where beneficial, namely during the intense mixing/heat exchange portion of a reaction, while more conventional modules like a coil or tubular heat exchangers are used afterward for an effective increase in volume.

In relation to heat exchange, three cases can be considered which are a function of the reaction rate (Type A, B, and C). For Type A reactions (millisecond to second), even with micro-structures, a hot spot can be formed and, in general, it is controlled via the multi-injection principle [10]. Organo-Grignard reactions are an example of intensely exothermic type A systems with a complex network of reactions that occur in the hot spot [11]. The Grignard reaction reported by Plouffe et al. [9], which shows a very high resolution in side-product formation as a function of the hot spot magnitude, makes it well suited to understand localized heat effects. It will be used here to further study different micro-reactor systems. Type B reactions have intermediate kinetics (between several seconds and minutes), but may still be fast enough to require significant heat exchange to reduce spatial variations in thermal conditions. A multi-scale approach is appropriate where the hydraulic diameter of a reactor is adjusted via a different plate or coil diameter depending on the local reaction kinetics (vide infra). Type C reactions have slower kinetics (between several minutes to hours) and can often be handled by conventional technology [9], except for cases with particularly hazardous chemicals or operating conditions.

The scale-up of production using micro-structures is often limited by the pressure drop, and a plate type reactor is generally more straightforward to scale up than a coil reactor. Figure 3.1 shows a Mix-Then-Reside (MTR) plate, where the initial mixing zone (in this case SZ) is the main contributor to the pressure drop of the plate. The hydraulic diameter of this mixing zone can be

adjusted for various flow rates via the 3/7th power rule as explained in [12]. On the other hand, upon scale-up, the residence time channel (RTC) may be enlarged in width (w) while the depth (d) is kept constant to maintain similar hydrodynamic conditions (and similar h_{in}) and hydraulic diameter leading also to a similar specific surface area for heat exchange (a). In fact, when such an approach is integrated into various sized-plates (A7, A6, A5…; Table 3.1, Figure 3.2), pressure drop can be kept reasonable for a single plate leading to high flow rates and productivity. Combined with a multi-scale approach, even longer residence times can be accommodated with the proper reactor unit while maintaining relatively low pressure losses. In other words, the size increase of a plate is consistent with the increase of volume (V) and surface area leading to a consistent scale-up, as opposed to the increase of the diameter of a coil; where a is inversely proportional to V.

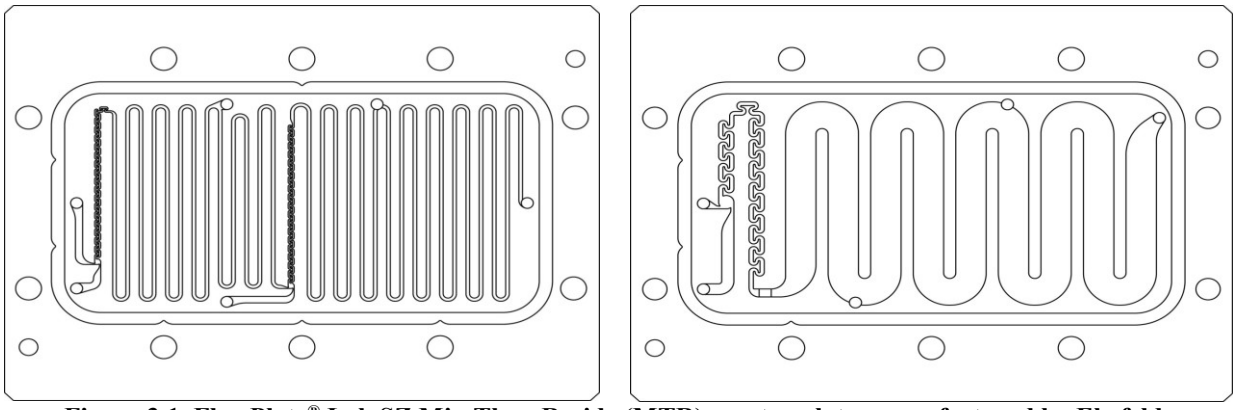

Figure 3.1. FlowPlate® Lab SZ Mix-Then-Reside (MTR) reactor plates manufactured by Ehrfeld Mikrotechnik BTS size 600 (left) and 300 (right)

Table 3.1. FlowPlate® sizes and production capacities

Plate Size	Flow Rate [mL/min]	Quantity*
FlowPlate® Lab (close to A7)	1.5-15	Development tool, few grams
FlowPlate® A6	15-150	6,500-65,000 kg
FlowPlate® A5	150-300	65,000-130,000 kg
FlowPlate® A4	300-600	130,000-260,000 kg

*Isolated product per year with product concentration from 10-100 wt% and density ~1000 kg/m^3

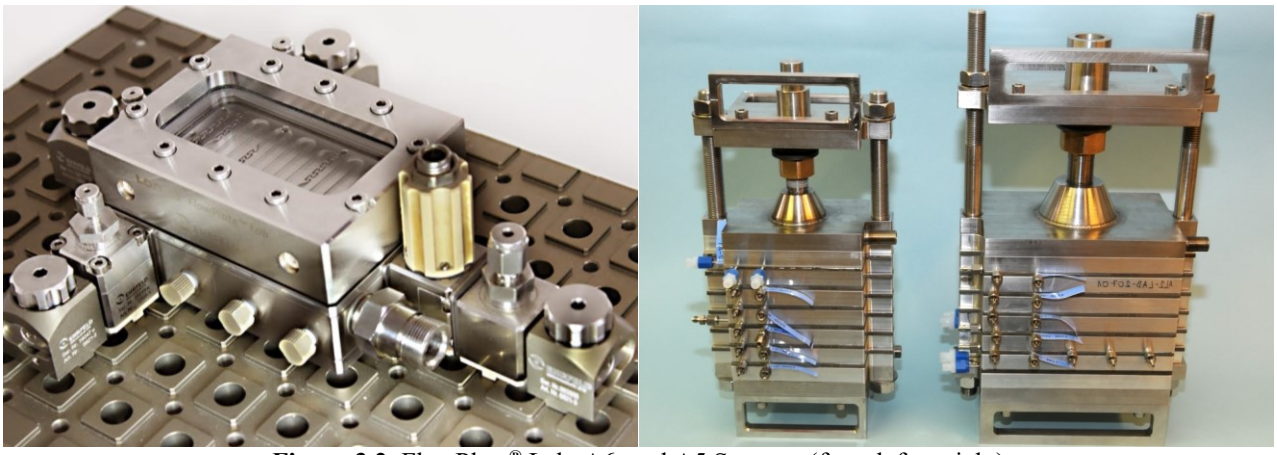

Figure 3.2. FlowPlate® Lab, A6, and A5 Systems (from left to right)

This work is focused on characterizing and developing models for the overall heat transfer performance of RTC plates and utilizing an exothermic test reaction to study the localized heat transfer in various MTR plates. The results are then used to understand the wall-to-fluid heat exchange capabilities and limitations of the plate micro-reactors for four different reaction case-studies.

3.1.1. Dimensionless Approach to Heat Transfer and Common Models

While it is generally accepted that the heat transfer in micro-reactors benefits from the inherent smaller length scales, the heat transfer performance is not fully understood, since a micro-channel is rarely a simple straight channel for which the classic wall-to-fluid heat transfer correlations were developed [13]. In order to study the heat transfer in the micro-channels, several dimensionless numbers are used, found in equations (3.1) to (3.4).

$$Nu = \frac{hD_h}{k_f} \tag{3.1}$$

$$Re = \frac{\rho u D_h}{\mu} \tag{3.2}$$

$$Pr = \frac{c_p \mu}{k_f} \tag{3.3}$$

$$Dn = Re\left(\frac{D_h}{2R_c}\right)^{1/2} \tag{3.4}$$

The Nusselt number (*Nu*) is the ratio of the convective to conductive heat transfer, where h is the convective heat transfer coefficient $[W/(m^2\,K)]$; D_h is the characteristic length of the channel – in this case, the hydraulic diameter $[m]$; and k_f is the thermal conductivity of the fluid $[W/(m\,K)]$.

The Reynolds number (*Re*) is the ratio of the fluid's inertial and viscous forces, where ρ is the fluid density $[kg/m^3]$; u is the fluid velocity $[m/s]$; and μ is the fluid's viscosity $[Pa\ s]$. The Prandtl number (*Pr*) is the ratio of the rates of viscous diffusion and thermal diffusion, where c_p is the fluid's heat capacity $[J/(kg\ K)]$. Lastly, the Dean number (*Dn*) is used to characterize flow in curved ducts, where R_c is the radius of curvature $[m]$.

For heat transfer studies in micro-reactors and micro-channels, there is little agreement in the literature on whether conventional, macro-scale correlations apply to the smaller scale systems [7,13–15]. Morini [14], as well as Steinke and Kandlikar [15], performed literature reviews on the available heat transfer data and found little consistency, concluding that further work is required in the field. Morini observed that when analyzing all data chronologically, the overall deviations between studies were decreasing. This trend was attributed to the technological improvements in the construction of the micro-channels, reducing the relative roughness and uncertainties in channel dimensions. Steinke and Kandlikar considered three key, underlying causes specific to research in micro-reactor systems responsible for the differences in various investigations [7,15]: the thermal entrance regions in relatively short micro-reactors; uncertainties in experimental measurements (e.g. small channel dimensions, wall temperatures, etc.); and ambiguity in the determination of the thermal boundary condition. These factors were taken into account when developing the experimental protocols used in this work.

For macro-scale systems in the fully developed laminar flow regime (Re<2,300), the Nusselt number is typically constant for straight channels [16]; while in the transitional (2,300<Re<10,000) and turbulent (Re>10,000) flow regimes, *Nu* can be described in terms of *Re* and *Pr*. Many studies claim that there is an early transition to turbulence in micro-channels; however, Steinke and Kandlikar showed that these studied did not account for developing flow or uncertainty in their calculations [15]. Nevertheless, due to the curvature of the micro-channels studied here, vortices can form, and secondary flow patterns can become chaotic at Reynolds numbers below typical transitional flow conditions [17–21], even when high aspect ratios (α) are employed [22]. These chaotic flow patterns are suspected to influence the Nusselt number in similar ways to turbulent flow, rather than Nu remaining constant, as in laminar flow. For this reason, several empirical Nusselt number correlations that are valid for transitional and turbulent flow regimes (Re>2300), regardless of boundary conditions [13], are considered, even though the

range of this study is 400<Re<2000. It is worth noting that the channels studied here in this range of Reynolds numbers can be considered hydraulically smooth, as the relative roughness is approximately 4×10^{-4} [23].

The Dittus-Boelter correlation was the simplest model considered where Nu_{DB} is a function of $Re^{0.8}$. This model is typically sufficient when the fluid properties can be assumed to be constant across the studied temperature range [13] and was developed for $0.6 \leq Pr \leq 160$ and $Re \geq 10{,}000$. The Sieder-Tate correlation (Nu_{ST}, valid for $0.7 \leq Pr \leq 16{,}700$ and $Re \geq 10{,}000$) extends upon this by incorporating a ratio between μ, the viscosity evaluated at the bulk temperature ($\overline{T_c}$), and μ_s, the viscosity evaluated at the surface temperature, T_s. This model is more accurate when there are larger temperature gradients in the system, as it accounts for the transport phenomena at the boundary conditions [13].

Lastly, the Gnielinski correlation (Nu_{Gn}) was considered because it is an accurate model for transitional and turbulent regimes since it incorporates a friction factor into its calculation, shown in equation (3.5). The Darcy–Weisbach friction factor, f, used in its calculation is given in equation (3.6), where ΔP is the pressure loss, in $[Pa]$, across the reactor length l, in $[m]$.

$$Nu_{Gn} = \frac{(f/8)(Re - 1000)Pr}{1 + 12.7(f/8)^{1/2}(Pr^{2/3} - 1)} \qquad \begin{bmatrix} 0.5 \leq Pr \leq 2{,}000 \\ 3{,}000 \leq Re \leq 5\times10^{6} \end{bmatrix} \tag{3.5}$$

$$f = \frac{2\,\Delta P}{\rho u^2}\left(\frac{D_h}{l}\right) \tag{3.6}$$

The Gnielinski correlation was developed for macro-scale applications, and Adams et al. showed that the correlation is sufficient in modeling Nu for non-circular channels with D_h as small as 1.2 mm [24]. They also showed that for smaller channel sizes, such as those studied here, a deviation factor can be applied to the Gnielinski correlation to achieve better predictions for Nu [25]. Although the Gnielinski model (with the deviation factor from Adams) would have been the preferred model, the term $(Re - 1000)$ would become negative for the range of flows that were studied, and this would not yield meaningful results. Therefore, a modified Gnielinski model will

be developed as in equation (3.7) where β and γ will be fit using the least squared error, ensuring that β is smaller than smallest Re studied (400).

$$Nu_{Gn} = \frac{(f/8)(Re - \boldsymbol{\beta})Pr}{1 + \boldsymbol{\gamma}(f/8)^{1/2}(Pr^{2/3} - 1)} \quad \textbf{(3.7)}$$

3.2. Experimental and Analytical Methods

3.2.1. Reactors Studied

3.2.1.1. RTC Plate used with a Non-Reactive System

The first investigation utilized an A6-sized FlowPlate® reactor manufactured by Ehrfeld Mikrotechnik BTS (Figure 3.3); namely the 320B, which is an RTC using half of the plate's area, shown in Figure 3.4. This RTC plate was chosen because it has a smaller operating volume with the same channel dimensions as the standard 321 RTC plate, which uses the entire A6 plate. The 'B' side was chosen over the 'A' side for ease of setup due to both inlet and outlet facing upwards, in addition to having more curves relative to the total volume, similar to the RTC sections on several MTR plates. The detailed dimensions of this plate can be found in Table 3.2. The RTC plate (in addition to the A5-sized plates used in the reactive system discussed below) was manufactured out of a 3.5 mm thick Hastelloy® C22 plate with a 1.5 mm plate welded to the other side; so, the metal's thickness is dependent on the channel's depth at that point. The thermal conductivity of Hastelloy® C22 is 10.9 $[W/(m\,K)]$ [26], significantly lower than that of Aluminium (273 $[W/(m\,K)]$ at 300 K) [23] with which the Heat Transfer Fluid (HTF) plates were made (new HTF plates are manufactured with copper with k=400 $W/(m\,K)$] [23]). The reactor plates and heat transfer fluid plates alternate in the FlowPlate® system, as shown in Figure 3.3. The HTF flow is operated in the turbulent regime at Reynolds numbers over 15000 to minimize the resistance to fluid-to-wall heat transfer in the HTF channel.

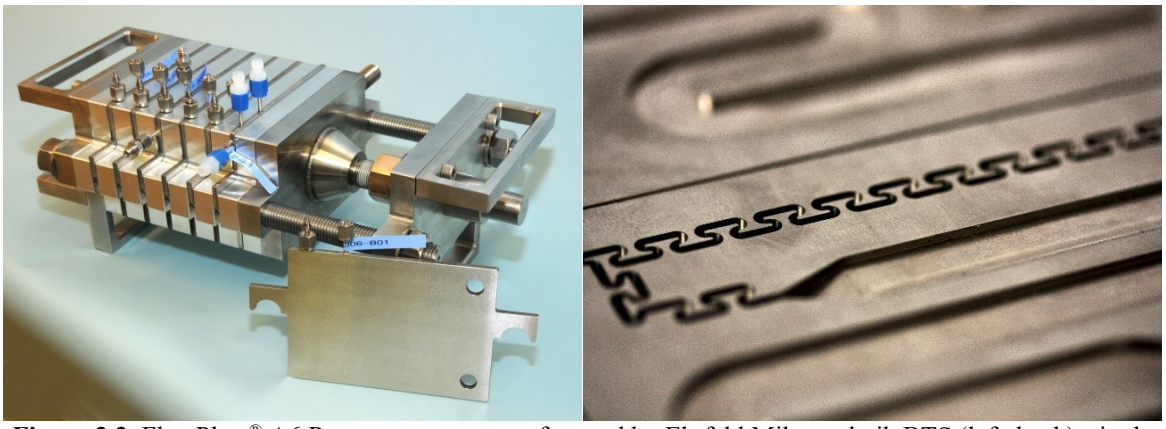

Figure 3.3. FlowPlate® A6 Reactor system manufactured by Ehrfeld Mikrotechnik BTS (left, back), single reactor plate (left, front), and an open MTR (SZ) reactor plate revealing the channels (right)

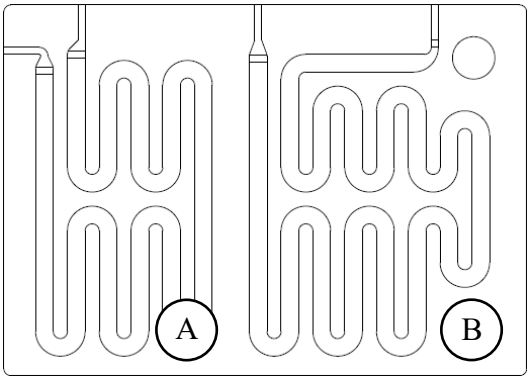

Figure 3.4. CAD drawings of the 320 RTC plate

Table 3.2. Reactor plate properties

Parameter	320B	315	215	240	260	350	[Units]
Plate size	A6	A6	A5	A5	A5	A5	
Plate material	Hastelloy®	Hastelloy®	Hastelloy®	Hastelloy®	Hastelloy®	SiC	
Plate Type	RTC	MTR	MTR	MTR	MTR	MTR	
Mixing Zone							
Mixer Type	-	SZ	SZ	TG	TG	TG	
Mixer Size	-	300	200	200	100	200*	
D_h	-	0.714	1.00	1.00	1.375	0.747	[mm]
w	-	0.5	0.7	0.7	1.0	0.7	[mm]
d	-	1.25	1.75	1.75	2.2	0.8*	[mm]
A_{ME}	-	4.61×10^{-5}	8.40×10^{-5}	8.84×10^{-5}	1.85×10^{-4}	6.50×10^{-5}	[m^2]
V_{ME}	-	6.74×10^{-9}	1.7×10^{-8}	3.96×10^{-8}	1.02×10^{-7}	1.81×10^{-8}	[m^3]
Specific area	-	6840	4890	2230	1820	3590	[m^2/m^3]
Residence Time Channel							
D_h	0.901	0.901	0.952	1.38	1.31	1.38	[mm]
w	5.0	5.0	10.0	5.0	10.0	5.0	[mm]
d	0.5	0.5	0.5	0.8	0.7	0.8	[mm]
l	617	-	-	-	-	-	[mm]
A_R	0.00679	-	-	-	-	-	[m^2]
V_R	1.54×10^{-6}	-	-	-	-	-	[m^3]
Specific area	4400	-	-	-	-	-	[m^2/m^3]
R_c	4.5	-	-	-	-	-	[mm]

*Not truly a size 200 due to reduced channel depth

3.2.1.2. MTR Plates used with a Reactive System

For the reactive system, the five MTR plates from Table 3.2 were used; each with a different mixer type (SZ or TG, as shown in Figure 3.5), scale (300, 200, or 100) or material (Hastelloy® C22 or SiC). Since the reaction is fast and occurs within a few milliseconds inside the reactor plate [9], it is only the geometry of a particular mixing-element that is of interest when comparing the five different plates. It is important to note that plate 350, the SiC TG plate, was custom built and has the HTF built into the plate (i.e. there is no contact resistance). The four other MTR plates fit into the FlowPlate® reactor system (either the size A5 or A6 rack, depending on plate) as with the non-reactive system described previously.

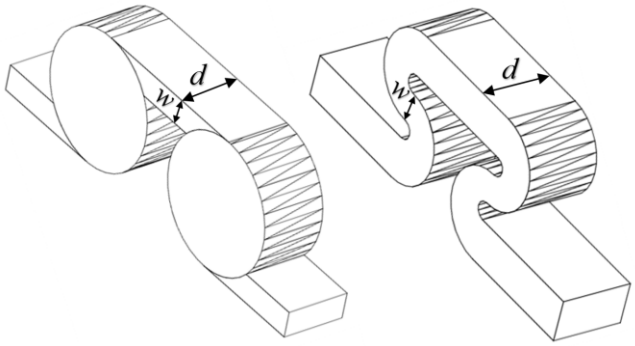

Figure 3.5. 3D representations of TG (left) and SZ (right) mixing elements

3.2.2. Heat Transfer Experiment Setup for Non-Reactive System

With reactor plates and heat transfer fluid plates alternating in the FlowPlate® system, heat is transferred to both sides of the plate. Two Huber Ministat 230 thermal baths were used; one cooled the reactor side feed down to 5 °C, while the other circulated hot water through the HTF channels at 90 °C. Two Syrdos syringe pumps from Hitec-Zang metered in the chilled water from the bath at the desired volumetric flow rates, while the hot thermal bath's internal pump circulated the hot water (measured by a calibrated in-line rotameter). Flow rates in the HTF plates ranged from 5.2-6.8 L/min and flow inside the RTC ranged from 27 mL/min to 110 mL/min. The standard range for the A6 plates used are generally from 15-150 mL/min; however, the lower flow rates reached thermal equilibrium with the HTF before the outlet (meaning no analysis was possible). At the higher flow rates, the internal resistance to convective heat transfer became too small of a fraction (<10%) of the total resistance, so the calculation of the Nusselt number contained significant error.

The overall setup used is shown in Figure 3.6. Note that the temperature was measured with four T-type thermocouples (Omega) at the inlet and outlet for both the reactor being studied ($T_{c,i}$ and $T_{c,o}$) and the HTF channels ($T_{h,i}$ and $T_{h,o}$). The pressure drop (ΔP) was also measured across the reactor using an Omegadyne PX409 0-17.5 bar differential pressure transducer to ensure no blockage was present in the channels and to measure the friction factor.

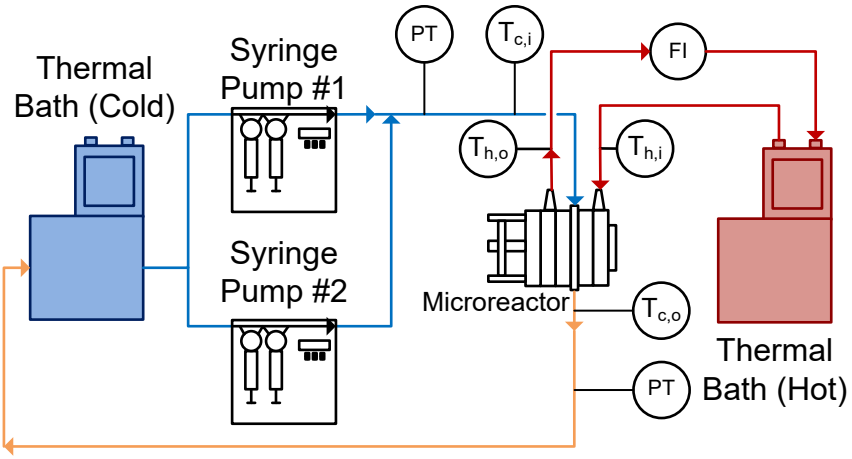

Figure 3.6. Schematic of heat transfer experimental setup

When assembling the FlowPlate® system, the plates were tightened to a torque of 15 $[N\ m]$, the specification given by the manufacturer. This was maintained for all experiments because this would significantly affect the contact resistance between the plates. A silver-based thermal paste purchased from McMaster-Carr was used to test the contact resistance. It was chosen due to its high thermal conductivity of (104 $[W/(m\ K)]$) in order to fill any gaps between the plates [27].

In order to insulate the system from the environment, a Styrofoam box was constructed with the required ports for the fluids to enter and exit the system, as well as the instrumentation wiring. The FlowPlate® A6 rack was in the box, surrounded by fiberglass insulation. This was done to ensure that the experiments were unaffected by the surrounding ambient temperature.

3.2.2.1. Water Properties at Temperatures Studied

The properties of water could not be assumed as constant throughout the reactor since this work was performed over a relatively wide range of temperatures (5-90 °C). The values for each property used at various temperatures are shown in Table 3.3 [28]. Note that, unless specified otherwise (e.g. viscosity at the wall temperature), the properties are evaluated at the average cold-side or hot-side temperatures, $\overline{T_c}$ and $\overline{T_h}$, respectively.

Table 3.3. Physical properties of water at various temperatures [28]

$\boldsymbol{Temperature}$ $[°C]$	$\boldsymbol{\rho}$ $[kg/m^3]$	$\boldsymbol{\mu}$ $[\times 10^4\ Pa\ s]$	$\boldsymbol{k}$ $[W/(m\ K)]$	$\boldsymbol{c_p}$ $[J/(kg\ K)]$
5	999.9	15.18	0.571	4205
25	997.0	8.900	0.607	4182
45	990.2	5.958	0.637	4180
70	977.7	4.035	0.663	4190
90	965.3	3.141	0.675	4205

3.2.3. Heat Transfer Setup for Grignard Reaction

At conditions similar to those presented in [9], the synthesis of methyl 2-oxobutanoate (2-MOB, **3**) was carried out in the MTR reactors from Table 3.2 using dimethyl-oxalate (DMO, **1**) and the Grignard reagent ethylmagnesium chloride (**2**). The reaction network is shown in Figure 3.7. Feed 1 consisted of 15 wt% DMO in dimethoxyethane (DME) and feed 2 had 19 wt% Grignard reagent, 58 wt% THF, and 23 wt% DME. Feeds 1 and 2 were maintained such that the ratio of Grignard:DMO remained 1.10 mol/mol. Both feeds were pre-cooled to the reactor's HTF temperature before mixing (either -5, -15, or -25 °C). The reaction was quenched with 1 mol/L HCl solution (HCl/Mg = 1.20 mol/mol) at the reactor outlet, and the yield was calculated as area percent from GC of **3** and the conjugated enol, **4**.

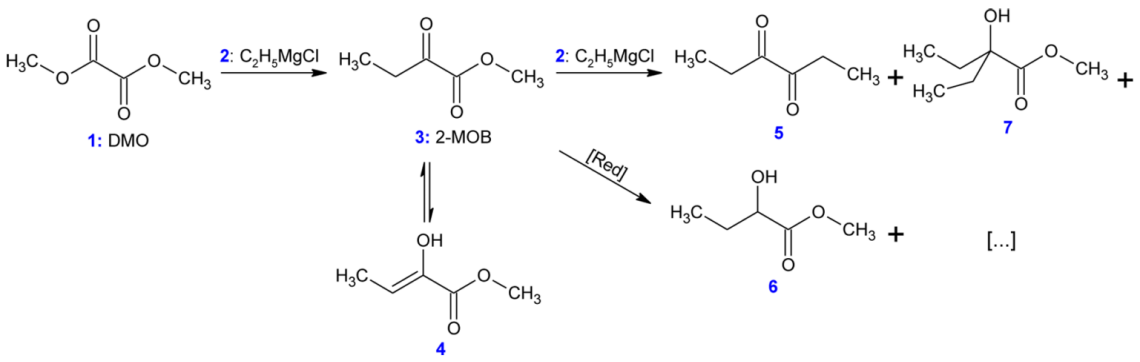

Figure 3.7. Reaction network for the synthesis of methyl 2-oxobutanoate (DMO)

3.2.4. Analytical Methods

3.2.4.1. Isolation of Nu from experimental data

In order to determine the Nusselt number for a given channel, an energy balance is performed on the cold stream (the inner channel). The energy gained by the cold stream (q_c) is equal to the heat transferred across the channel wall (q_w) as defined by equations (3.8) and (3.9), respectively.

$$q_c = \dot{m} c_{p,c} (T_{c,o} - T_{c,i}) \tag{3.8}$$

$$q_w = U A_{HE} \Delta T_{LM} \tag{3.9}$$

Where $\dot{m}$ is the mass flow rate (in $[kg/s]$); c_p is the heat capacity of the cold stream (in $[J/(kg\ K)]$); $T_{c,i}$ and $T_{c,o}$ are the fluid inlet and outlet temperatures, respectively; UA_{HE} is the product of the overall heat transfer coefficient and area available for heat transfer across the wall (in $[W/K]$); and ΔT_{LM} is the log mean temperature difference defined in equation (3.10). Since the HTF follows a serpentine path on either side of the reactor plates in opposite directions, it cannot be assumed to be either co-current or counter-current. However, the HTF flow is sufficiently high (as will be shown) and less than 1 °C is lost; allowing for the approximation of constant HTF temperature at $\overline{T_h}$ (the average hot side temperature).

$$\Delta T_{LM} = \frac{\Delta T_{w,o} - \Delta T_{w,i}}{\ln\left[\frac{\Delta T_{w,o}}{\Delta T_{w,i}}\right]} = \frac{T_{c,i} - T_{c,o}}{\ln\left[\frac{\left(\overline{T_h} - T_{c,o}\right)}{\left(\overline{T_h} - T_{c,i}\right)}\right]} \tag{3.10}$$

After equating equations (3.8) and (3.9), it is possible to calculate UA_{HE} for every experimental point. To isolate the convective heat transfer coefficient of the inner channel, h_{in}, the system is expressed in terms of thermal resistances as a thermal circuit in Figure 3.8. The total thermal resistance, R_{tot}, or $1/UA_{HE}$, is plotted vs. $1/Re_{in}$. When Re_{in} approaches infinity, the thermal resistance due to internal convection, $R_{conv,in}$, approaches zero. The intercept of the plot of $1/UA_{HE}$ vs. $1/Re$ is therefore equal to R_{ext}; which is the sum of all thermal resistances between the hot and cold streams excluding $R_{conv,in}$. h_{in} (and therefore Nu) can now be calculated using equations (3.11) to (3.13) at each data point by calculating the constant R_{ext} for a given data set. While the resistances to conduction through the plate walls are constants determined by the thickness and thermal conductivity of the metal, it is possible to manipulate the resistance due to convection in

the heat transfer fluid ($R_{conv_{out}}$) and the contact resistance between the aluminium and Hastelloy® C22 plates ($R_{contact}$).

$$R_{conv,in} = R_{tot} - R_{ext} = \frac{1}{h_{in}A_{HE}} \tag{3.11}$$

$$R_{tot} = 1/UA_{HE} \tag{3.12}$$

$$R_{ext} = R_{conv,out} + R_{cond_{HTF\ Plate}} + R_{contact} + R_{cond_{MR\ Plate}} \tag{3.13}$$

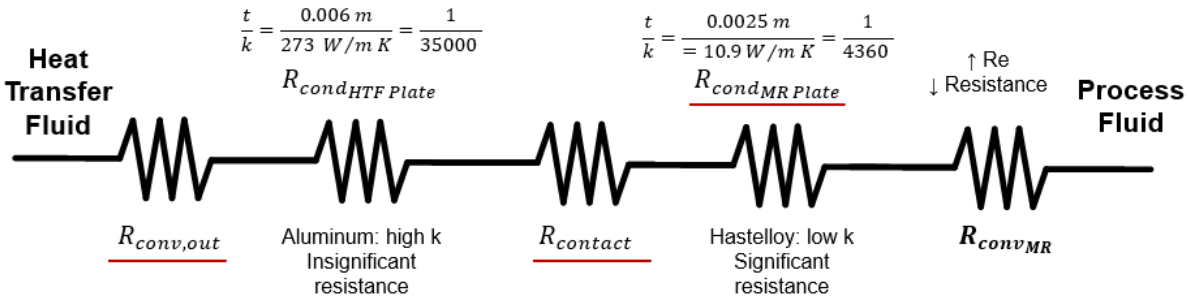

Figure 3.8. Thermal circuit diagram between heat transfer fluid and process fluid; highlighting potentially significant external resistances in red

3.3. Results and Discussion

3.3.1. Residence Time Channel (RTC) Heat Transfer Modeling

As previously mentioned, when the flow rate is increased in a system with alternating (right/left) curved channels, the Dean vortices can become chaotic while Re is still below 2300 [17]. This is the case with the results presented, as evident in the pressure loss and friction factor results for the entire plate (including inlet/outlet) vs. Re shown in Figure 3.9. Fitting the friction factor results to a model as in equation (3.14) is applicable due to localized regions of chaotic flow in the bends [17]. This yields a f_c of 0.105, which accounts for 25-50% of the total friction factor for the lowest and highest flow rate studied, respectively, indicating that a heat transfer model that accounts for transitional/turbulent flow may fit the results. While turbulent flow is often associated with a constant friction factor, this is not the case with hydraulically smooth pipes where the friction factor is still decreasing at Reynolds numbers above 10^8 [23]. It is due to the changing nature of the observed friction factor that the Gnielinski model was used as a basis to model the heat transfer in the RTC.

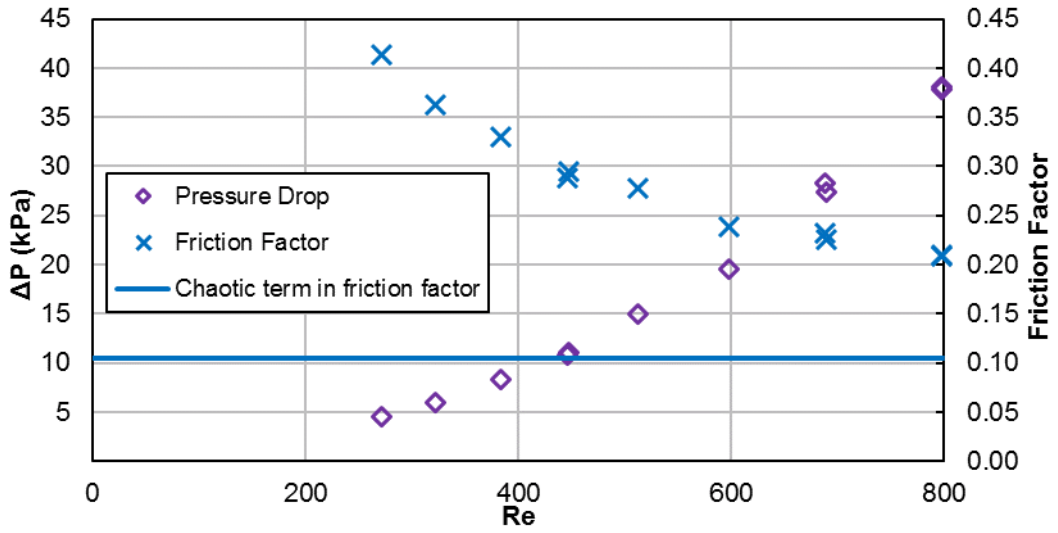

Figure 3.9. Pressure loss and friction factor vs. Re for the 320b RTC

$$f = f_c + \frac{f_l}{Re} \tag{3.14}$$

The raw temperature data from various experiments is presented in Figure 3.10. The HTF temperature (the theoretical maximum for any reactor plate outlet temperature) is the average of the inlet and outlet temperatures to the jacket side, which ranged no more than 1 °C. The inlet temperature varied with flow rate because of the syringe residence time before entering the insulated system.

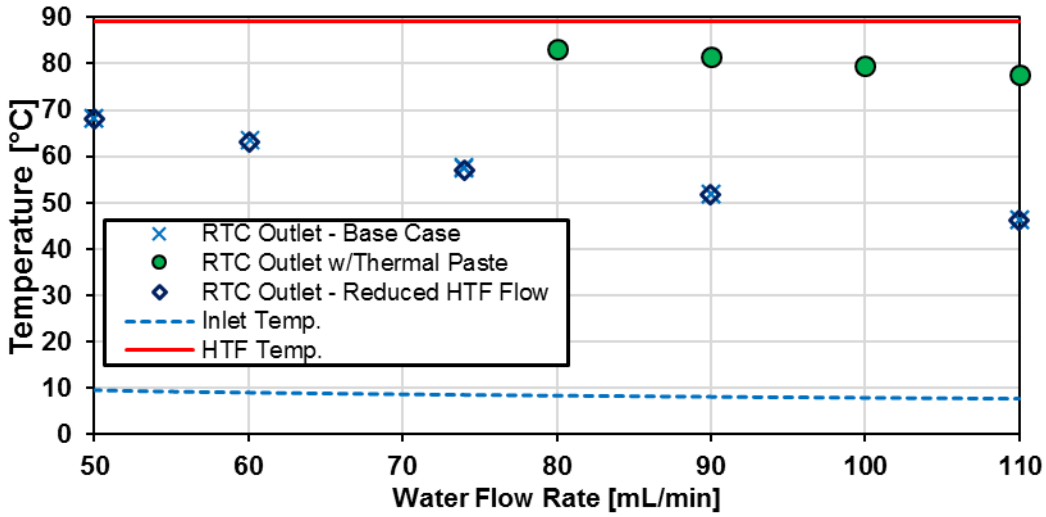

Figure 3.10. Temperature vs. internal water flow rate for various conditions for the 320B-RTC

3.3.1.1. RTC Base Case

The base case for the RTC uses no thermal paste between the HTF and RTC plates. It also uses the maximum HTF flow rate available, 6.8 $[L/min]$. The external resistance used for the calculation of h_{in} and Nu as in equation (3.11) can be seen in the base case results in Figure 3.11 when Re approaches infinity at the intercept where 1/Re is equal to zero. Note that the external resistance accounts for 85-90% of the total resistance. This can be significantly reduced, as discussed in section 3.3.1.2, but these conditions were required to obtain reliable Nu numbers (internal convection) with sufficient experimental points, and ΔT (see Figure 3.10).

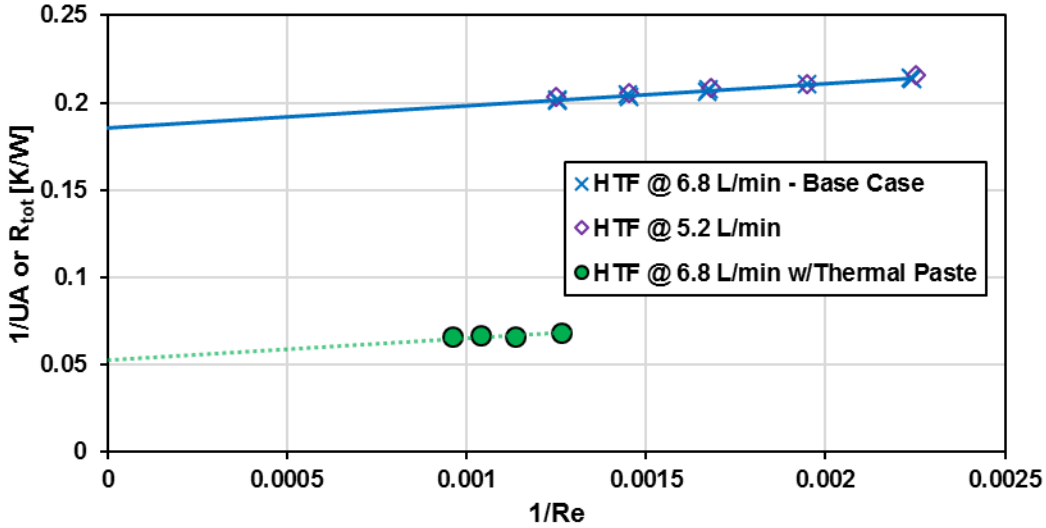

Figure 3.11. Total thermal resistance vs. 1/Re

The base case results from Figure 3.11 can be used to calculate the experimental Nusselt number, as shown in Figure 3.12. Applying a least squares fit to the model from equation (3.7) yielded values of 141 and 18.5 for β and γ, respectively. Clearly, the Nusselt number is not constant with respect to Re as predicted by laminar flow in a straight channel; indicating that the primary mechanism of heat transfer is from turbulent eddies generated in the channel's curvature. Indeed, when fitting the Nu results to a Sieder-Tate type model, the exponent for Re is 0.85 ± 0.12 compared to the expected value of 0.8 for turbulent flow (as used in equation (3.16)).

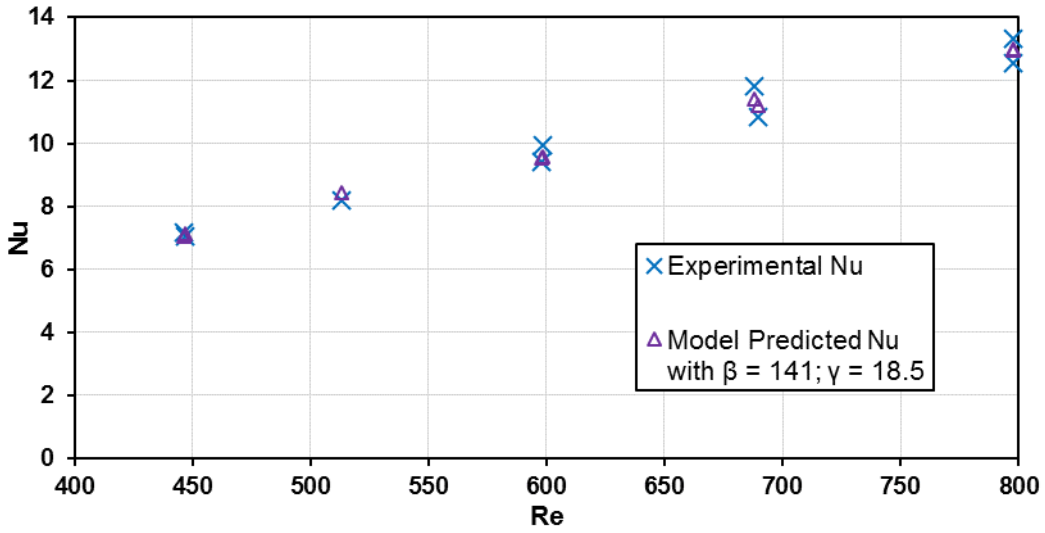

Figure 3.12. Nusselt number (experimental and predicted) vs. Reynolds number for the 320b RTC

3.3.1.2. Reduction of External Resistances in the FlowPlate®

This reactor's technology was designed to minimize the external heat transfer resistance so that the main contribution comes from the internal resistance to convection. One approach is to operate with a large excess of thermal fluid in an isolated loop to minimize thermal losses. The intention is not optimized heat exchange efficiencies in a counter-current mode, but rather a rapid temperature homogenisation to avoid localized hot spot formation due to reactions. In such a case, the design of the thermal fluid channel did not need to be micro-structured but was instead designed for operation in the turbulent regime to maximize heat transfer capability. The typical Re number (with water as HTF and flow rate of 6.8 $[L/min]$) is 15000. The HTF channel geometry of the FlowPlate® A6 or A5 is intended to be used for the delivery of thermal fluid from major laboratory brand of cryostats (Huber, Julabo, etc.). The HTF plates have the additional advantage of using aluminum or copper (high k metals) because the chemical compatibility is not an issue as in the reactor plates (which use Hastelloy® C22).

As previously noted, the external resistance was relatively high compared to the internal resistance to convection. To ensure $R_{conv,out}$ is minimized, the HTF flow rate must be increased towards infinity; however, the thermal bath was already operating at maximum flow rate (6.8 $[L/min]$). To determine if the external convective resistance had a significant effect on R_{ext}, the thermal fluid flow rate was decreased to 5.2 $[L/min]$. If reducing the HTF flow raised the total resistance compared to tests with the maximum flow rate, it would indicate that $R_{conv,out}$ still represents a

significant portion of R_{tot}. Figure 3.11 shows that reducing the HTF flow rate had a negligible effect on the total resistance, and $R_{conv,out}$ can be considered marginal for these operating conditions.

A silver-based thermal paste was applied between the reactor and heat transfer plates to fill any voids with highly conductive paste to reduce the contact resistance between the plates. When performing these tests, the observed UA_{HE} was around 15 $[W/K]$, leading to a U of 2200 $[W/(m^2\ K)]$ when using the internal area available for heat transfer from Table 3.2. Note that almost all the flow rates tested resulted in the internal fluid reaching thermal equilibrium with the HTF before the outlet, as seen in Figure 3.10, meaning they cannot be used in the Nusselt number analysis. However, the silver-based thermal paste evidently reduced the external resistance by around 70% with the few points that could be studied in Figure 3.11, and thermal paste will substantially increase the rate of heat transfer between the plates. Indeed, if you were to use the same slope as the base-case results (where there was enough resolution to measure the internal convection), the external resistance is estimated to be 0.05 $[K/W]$ in these tests. Though this resistance, which is basically the sum of material and remaining contact resistances still contributes to ca. 80% of the overall resistance to heat transfer under the flow rate studied. The next section will introduce a test reaction that can further study this aspect.

3.3.2. Test Reaction to Study Localized Heat Transfer

The Grignard-type homogenous synthesis of methyl 2-oxobutanoate (2-MOB, **3**) from dimethyl-oxalate (DMO, **1**) and ethylmagnesium chloride (**2**) was used to test several plate reactors. Since the reaction yield is such a strong function of temperature, it is a useful test reaction for understanding localized heat transfer. First, tests were performed in the 240 plate with either one or two injection points to demonstrate the Grignard reaction's high sensitivity to temperature hotspots along the length of the channel. Since there are competitive reactions that are favoured at higher temperatures, it is important to keep the temperature as low as possible. This can be challenging due to the exothermic nature and very fast kinetics of the reaction, causing hotspots to form in the mixing zone of the injection points. Figure 3.13 clearly shows that reducing the local concentration of one reactant by injecting it at two points along the channel length increases the overall yield versus one single addition at the plate reactor inlet. In previous work, we have demonstrated that this effect is not a contribution of better mixing but that it is essential to return

the fluid temperature near the sink level of the thermal fluid before the next injection point [11]. With half of the reactant available, the total heat released near the inlet is about halved, favouring the main reaction over its competitive reaction to produce **5** or **7** from Figure 3.7.

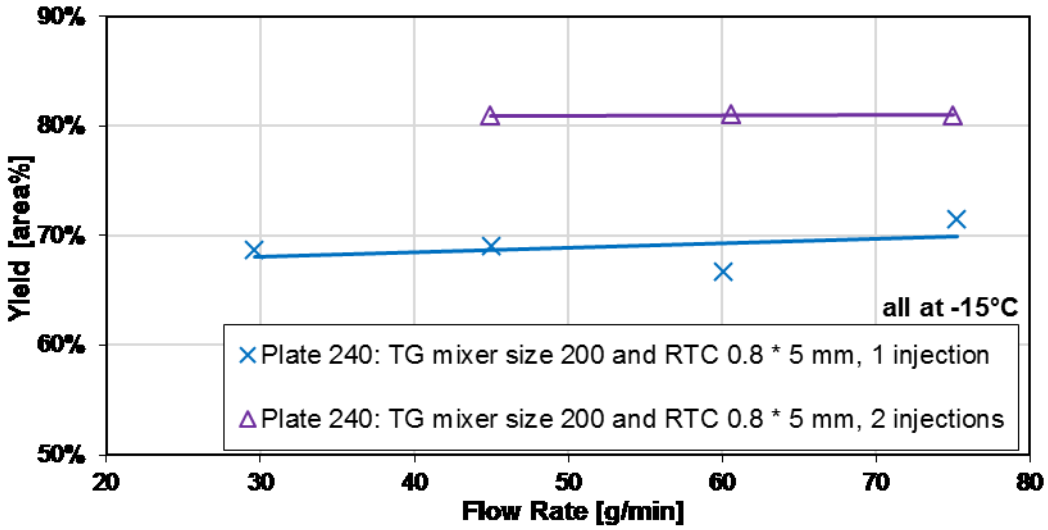

Figure 3.13. Effect of multi-injection for Grignard Reaction

The temperature effect itself can be observed when comparing the same reaction at multiple temperatures for two different plates. Shown in Figure 3.14, the reactions with lower overall temperatures resulted in higher yields. Although two separate plates were used with different dimensions, the 10°C temperature changes resulted in a similar difference in yield, but the main factor to control yield remains the multi-injection approach.

Note that the product yield is only slightly positively correlated with flow rate for the range studied since various counteracting factors are involved. Assuming the reaction is fully mixing controlled, four cases can be depicted: (1) an increase of flow rate favors mixing via higher energy dissipation rate leading to better selectivity (higher yield) for reactions encompassing parallel-consecutive pathways; (2) better mixing also means reagents react in a shorter time (i.e. in a smaller flow path), releasing the heat in a more confined volume which intensifies the hot spot (lowering the yield); (3) the increase of flow rate also increases the reaction heat intensity (power) leading to a larger hot spot; (4) this effect is however somehow counteracted by the decrease of internal heat resistance. It is this sensitive impact of temperature on selectivity that allows this reaction to be a useful tool for the detection of hotspots in reactors.

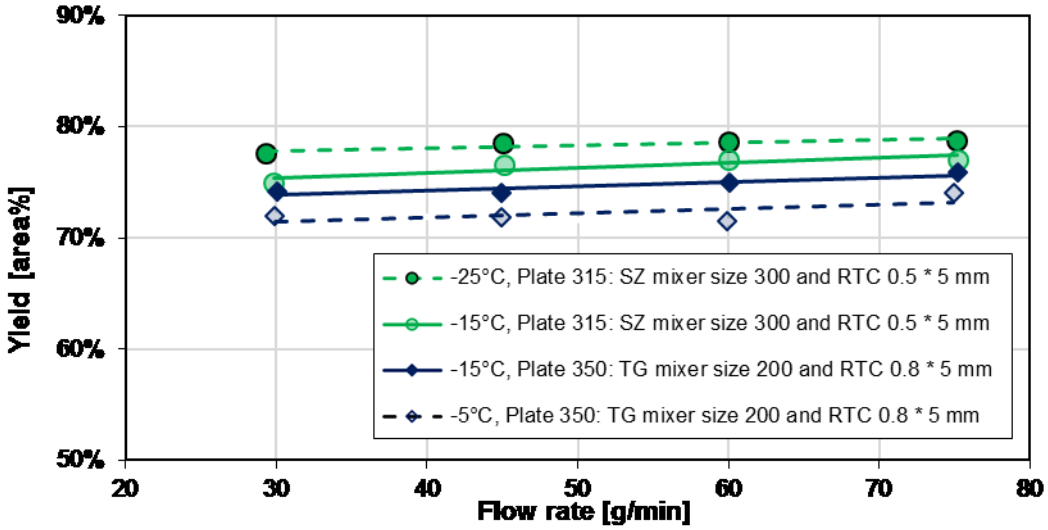

Figure 3.14. Yield vs. flow rate in the 315 and 350 plates at various temperatures

Figure 3.14 is also comparing two different reactor plates in size and material at the same temperature (-15°C) and one could potentially conclude that the smaller size (Plate 315) plays a more predominant role to favor heat exchange than the highly heat conductive material (Plate 350). The situation is, however, more complex, and it was not possible to get identical plates out of different materials due to various manufacturing methods. One of the issues comes from the fact that when the mixer size is changed, the mixing efficiency is also altered accordingly and we know from the impact of flow rate that mixing plays a certain role (vide supra). In other words, the mixer specific surface area (a) and the mixing intensity (u^3/d_h; specific energy dissipation rate) are confounded factors. Fortunately, there were four geometrically different Hastelloy plate reactors that could be tested under identical conditions, and these results are shown in Figure 3.15 (a) and (b). A linear trend is observed between the metallic plates, with the SiC reactor being clearly an outlier with slightly better performance. Thus, one can now conclude that a plate reactor with a more heat conductive material and no contact resistance will have better yields.

In summary, the selected Grignard test reaction had sufficient resolution to differentiate between plates made from different materials and contact resistances. It was not possible to decouple the effect of geometry from the mixing intensity, as both factors are confounded and further simulations are required to reach this goal. All in all, the multi-injection principle is the most important factor to control the hot spot, followed by feed concentration [9] and temperature. The plate material, the contact resistance, the mixing intensity, and the specific surface area are

additional factors with less importance that control the extent (peak magnitude and broadness) of the hot spot.

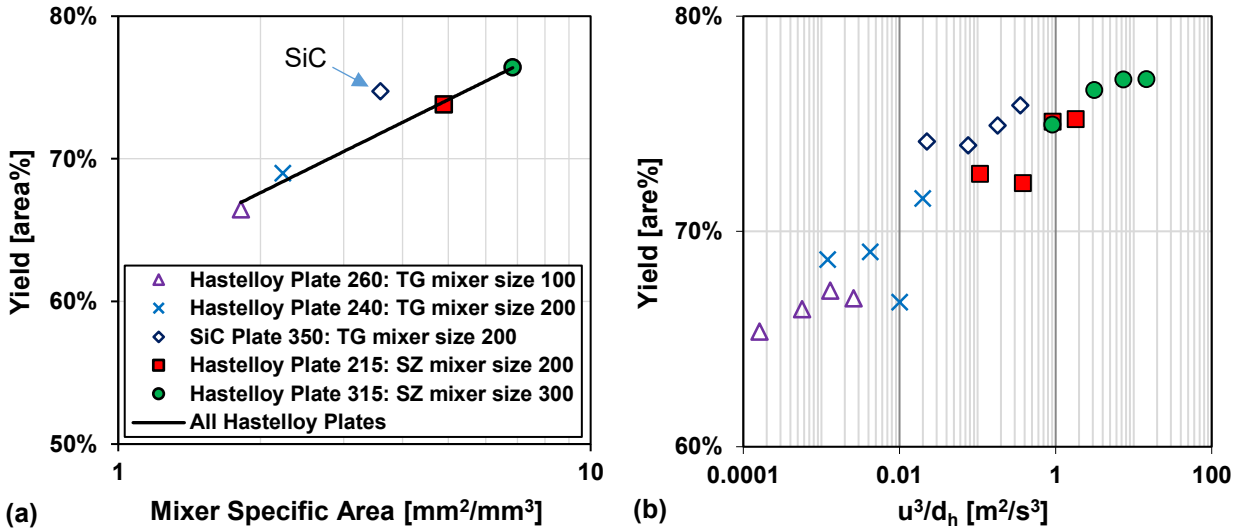

Figure 3.15. (a) Average Grignard reaction yield (at -15 °C) vs. mixer specific area for heat transfer, and (b) Grignard reaction yield (at -15 °C) vs. specific energy dissipation rate (u^3/d_h)

3.3.3. Case Studies on Plate Reactor Heat Transfer Capabilities

The purpose of this study was to evaluate the micro-reactors for applications requiring significant heat removal/addition for exo/endothermal reactions. The enhanced wall-to-fluid heat transfer rates provided by micro-reactors' high area-to-volume ratio enable reactions that generate or consume large amounts of heat and the use of more concentrated reactants while greatly reducing the potential of a thermal runaway. The thermal control performance of a reactor as a whole can be expressed using the fourth Damköhler number, Da_{IV} in equation (3.15). This dimensionless number represents the ratio of heat generation, calculated from the reaction rate r, the reaction enthalpy ΔH_R and the reactor volume V_R, to heat transfer in the reactor, calculated from the overall heat transfer coefficient U, the total area for heat transfer, A_{HE}, and the temperature driving force ($|T - T_{TF}|$) between the reactive media and thermal fluid used to control the temperature. This number considers all the parameters necessary to optimize the heat transfer in a system. To be satisfactory, this ratio is ideally smaller than one.

$$Da_{IV} = \frac{q_{rxn}}{q_{HE}} = \frac{|r\Delta H_R| \cdot V_R}{UA_{HE}(|T - T_{TF}|)} \ll 1 \qquad \textbf{(3.15)}$$

For a given reaction, this can be achieved independently of the reactor scale by lowering the reaction rate using diluted solutions and/or colder temperatures, but these options go against the philosophy of process intensification, and a particular temperature or concentration may be required for yield optimisation. Alternatively, the temperature of the thermal fluid can be adjusted, but this cannot realistically impact Da_{IV} by much more than one order of magnitude.

The remaining parametric options, U, A_{HE} and V_R, all vary with scale. As discussed, the overall heat transfer coefficient is a function of the internal convective resistance to heat transfer as well as the external resistances in the system (metallic wall conductive and contact resistances, and thermal fluid side convective resistance), which are impacted more so by the system setup rather than scale. The reactor side convection coefficient, h_{in}, will not vary greatly with the scale-up as shown in equations (3.16) (a Sieder-Tate-like model that was fit with the results from Figure 3.12) and (3.17). Note that the ratio Q_2/Q_1 of equation (3.17) is changed into a hydraulic diameter ratio using the 3/7th scale-up rule based on constant energy dissipation rate (ε) [12].

$$h_{in} = Nu_{in}\frac{k}{D_h} = A \cdot Re_{in}^{0.85} \cdot Pr^{0.33} \cdot \frac{k}{D_h} \tag{3.16}$$

$$\frac{h_{in,2}}{h_{in,1}} \propto \left(\frac{Re_{in,2}}{Re_{in,1}}\right)^{0.85}\left(\frac{D_{h,1}}{D_{h,2}}\right) = \left(\frac{Q_2}{Q_1}\cdot\frac{D_{h,1}}{D_{h,2}}\right)^{0.85}\left(\frac{D_{h,1}}{D_{h,2}}\right) = \left(\left(\frac{D_{h,2}}{D_{h,1}}\right)^{\frac{7}{3}}\right)^{0.85}\left(\frac{D_{h,1}}{D_{h,2}}\right)^{1.85} = \left(\frac{D_{h,2}}{D_{h,1}}\right)^{\frac{7}{3}(0.85)-1.85} \approx 1 \tag{3.17}$$

The ratio between the area available for heat transfer, A_{HE}, and the reactor volume, V_R, is dependent solely on the D_h of the channels as shown in equations (3.18) and (3.19).

$$D_h = \frac{2dw}{d+w} \tag{3.18}$$

$$\frac{A_{HE}}{V_R} = \frac{2(d+w)l}{dwl} = \frac{4}{D_h} \tag{3.19}$$

Using the thermal paste case with the 320B RTC; Figure 3.11 shows that the overall heat transfer coefficient, U, is roughly equal to $2200\ [W/(m^2\ K)]$. A common heat exchanger design heuristic [29] uses 10 K as the minimum approach temperature, $|T - T_{tf}|$. Using this value, is possible to plot the Da_{IV} as a function of the hydraulic diameter for various volumetric heat generation rate $r\Delta H_R$. The Da_{IV} of four case studies are evaluated and discussed below. Each case can be

classified as a reaction and phase type described by Plouffe et al. based on their kinetics [9]. These are displayed on Figure 3.16 along with the RTC channel size used in this work ($D_h = 909$ $[\mu m]$).

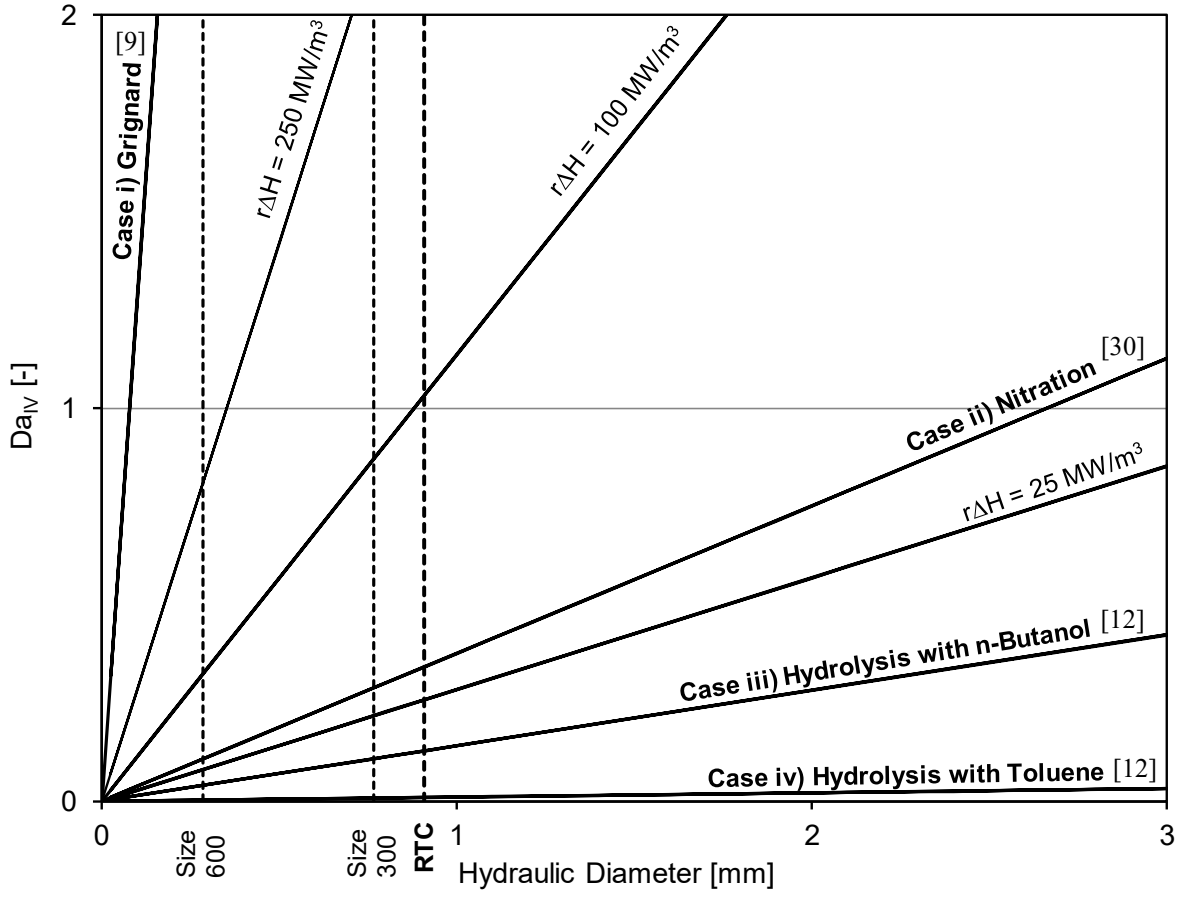

Figure 3.16. Fourth Damköhler number at different heat generation rates as a function of the sized-up hydraulic diameter and with U = 2200 W/(m^2 K) and |T-T_{tf}| = 10 K

3.3.3.1. Case i) Grignard Reaction

The first case study, case i), is the Grignard used in section 3.3.2. The reaction enthalpy change is approximately 225 $[kJ/mol]$ at -15 ºC and it is reasonable to assume that the reaction is completed within the first 100 milliseconds in the plate reactor (i.e., Type A reaction) [9]. This corresponded to an average reaction rate of ~5000 $[mol/(m^3\ s)]$ and to a heat generation rate $r\Delta H_R$ of 1125 $[MW/m^3]$. The necessary hydraulic diameter to avoid a temperature spike would need to be below 80 $[\mu m]$ – below the smallest dimension presented in this work. An alternate solution is to distribute the Grignard reactant along the plate reactor volume using multiple inlet ports (multi-injection approach) as previously shown; either with a plate with multiple ports, or multiple plates

in series. This multi-injection approach is of course also possible with conventional technology (i.e., not micro-structured) but with reduced process intensification capabilities.

3.3.3.2. Case ii) Nitration

The second case study, ii), is the homogenous nitration of salicylic acid using a solution of acetic and nitric acid. The experimental details are described again in [9]; the reaction needs to be operated at 65 ºC or above to avoid delays associated with the auto-catalytic behaviour of the reaction. At this temperature, the reaction rate was estimated to be ~230 $[mol/(m^3\ s)]$ (type B), and the reaction enthalpy is 146 $[kJ/mol]$[30], which yielded a heat generation rate of 33 $[MW/m^3]$. This is sufficiently low to be operated in micro-reactors, but not necessarily in milli-structures with internal diameters greater than 2.5 $[mm]$. Upon scale-up, it would then be best to use an adaptive channel design starting at a small size where the reactants meet and where the heat generation is high, and progressing into larger channels as the reaction rate decreases, i.e., maintaining the value $\frac{rV_R}{A_{HE}}$ constant (multi-scale approach). Typically, a plate with a channel depth starting in the micrometer domain will be selected and increased in size until conventional and readily available heat transfer technology can be used.

3.3.3.3. Cases iii) and iv) Two-Phase Hydrolysis

The third and fourth case studies are the liquid-liquid hydrolysis reaction commonly utilized for the characterization of micro-reactors for liquid-liquid mass transfer [12,31–36]. While the hydrolysis step itself is not highly exothermic, it is followed by two neutralization steps that result in an overall enthalpy change of about 112 $[kJ/mol]$. The cases here considered the use of a 0.5 mol/L solution of the acetate in drop flow operated at an energy dissipation rate of ~100 $[m^2/s^3]$. Under homogenous conditions, the initial reaction rate would be 3500 $[mol/(m^3 s)]$ (type A) and the total heat release rate at around 390 $[MW/m^3]$. However, these liquid-liquid cases have the distinction of being interphase mass transfer limited, which reduces the observed reaction rate, r. The rate constant is instead equal to the dispersed phase overall volumetric mass transfer coefficient.

Case iii) analyzes the use of n-butanol as the organic solvent. At these conditions, the coefficient $K_d a$ was $2.22 \cdot 10^{-1}$ $[s^{-1}]$ [12], which would result in an initial reaction rate of ~110 $[mol/(m^3\ s)]$ and a heat generation rate $r\Delta H_R$ of 12.5 $[MW/m^3]$. Clearly, the results indicate that a micro-

structure is no longer needed for the control of reaction heat (as it is safe to operate at a D_h below 7 $[mm]$), but rather to increase the rate of mass transfer to increase the overall rate of reaction.

The fourth case considers the use of toluene instead of butanol as the organic solvent. In such case, the coefficient $K_d a$ is reduced to $1.66 \cdot 10^{-2}$ $[s^{-1}]$ [12] and the heat generation rate $r\Delta H_R$ to 0.9 $[MW/m^3]$.

Low heat generation rates such as in case iv) can be safely operated in a channel with internal diameters below 90 $[mm]$. However, under the flow rates studied in this work, the energy dissipation rate in such a large reactor would be very low and the system even more mass transfer limited. The use of a micro-reactor for fast liquid-liquid reactions was necessary to obtain interphase mass transfer rates that are greater than what would be achieved in larger reactor.

Even at high energy dissipation rates using toluene, the acetate hardly transferred to the aqueous phase due to its affinity with the organic solvent (demonstrated by its high partition coefficient H_A). Consequently, large residence times are still needed and cannot realistically be achieved in micro-reactors within reasonable pressure drops. For example, at energy dissipations rates of 100 $[m^2/s^3]$, the overall volumetric mass transfer coefficient $K_d a$ with toluene was such that to obtain a conversion of 90%, a residence time of about 60 seconds would be needed and would result in a pressure drop of 60 $[bar]$ ($\Delta P = \rho \varepsilon \tau$) [12].

In such cases and when heat transfer is not limiting, reactors combining larger channels with an active mixing technique might present the best solution. Active mixing techniques use an external source of energy to agitate the fluids such as mechanical actuators. The energy dissipation rates that can be achieved are generally independent of the overall flow rates, and thus high values can be obtained at the same time as large residence times and low pressure drops. The use of pulsating flow in reactors with baffles [37] or without [38] have been proven to be useful tools in these cases.

3.4. Conclusions

Non-reactive heat transfer experiments were performed in the A6-sized FlowPlate® system manufactured by Ehrfeld Mikrotechnik BTS. For a residence time channel with Reynolds numbers ranging from 400-2000, the internal Nusselt number was fit to a Gnielinski-like model. This was deemed appropriate due to the curvature in the channels. The channel's curvature could form chaotic eddies at relatively low Reynolds numbers, which agreed with the observed friction factor

results. The Nusselt number also correlated with Reynolds to the power of 0.85 ± 0.12, which is similar to that of the turbulent Sieder-Tate correlation (0.8); further confirming the use of a model in transitional/turbulent flow over laminar flow. The external resistances to heat transfer were also studied in this system; specifically, the HTF flow rate and the contact resistance between the HTF plate and RTC plate. The largest contributor to the resistance of heat transfer was shown to be the contact resistance, which could significantly reduce the external resistance (by approximately 70%) using a silver-based thermal paste.

A test reaction, the synthesis of methyl 2-oxobutanoate using dimethyl-oxalate and the Grignard reagent ethylmagnesium chloride, was also presented as a means to differentiate localized heat transfer characteristics in various micro-mixer shapes, materials, injection ports, and scales. Due to the fast reaction kinetics, high exothermicity, and the increased selectivity for the desired product at lower temperatures, this reaction allows for a semi-quantitative comparison of hotspot formation in different plate reactors when comparing total yields. It was shown that the Grignard reaction can be used as a sensitive tool to compare different reactors when the specific heat transfer parameters are not fully known. As predicted by heat transfer theory, a multi-injection approach was the most effective method for reducing the magnitude of hotspot formation, thereby increasing the reaction yield. Additionally, increasing the specific area of a mixer geometry led to higher yields due to increased wall-to-fluid heat transfer.

Lastly, four case studies were analyzed based on the fourth Damköhler number to evaluate what maximum channel diameter would allow sufficient heat removal based on the overall heat transfer coefficients found experimentally. With a known reaction rate and heat of reaction, it is possible to select a suitable channel size. This analysis is a useful addition to the toolbox developed by Plouffe et al. [9] when selecting a proper reactor system for a given application.

3.5. Nomenclature

Symbols		$[Units]$
General		
a	Specific area (single phase) or specific interfacial area (biphasic)	$[m^2/m^3]$
A_{HE}	Area available for heat transfer	$[m^2]$
c	Empirical constant for calculation of thermal developing region	$[-]$
c_p	Heat capacity of fluid	$[J/(kg\ K)]$
d	Contraction depth	$[m]$
D_h	Hydraulic diameter at contraction $(2wd/(w+d))$	$[m]$

Da_{IV}	Damköhler Number	$[-]$
Dn	Dean number	$[-]$
f	Friction factor (Darcy–Weisbach definition)	$[-]$
f_c	Chaotic term in friction factor	$[-]$
f_l	Laminar term in friction factor	$[-]$
h	Local convective heat transfer coefficient	$[W/(m^2K)]$
H_A	organic/aqueous concentration distribution coefficient	$[-]$
ΔH_r	Reaction enthalpy change	$[J/mol]$
HTF	Heat Transfer Fluid	
k	Thermal conductivity	$[W/(m\,K)]$
K_d	Overall convective mass transfer coefficient (m/s)	$[m/s]$
l	Reactor Length	$[m]$
$\dot{m}$	Mass flow rate	$[kg/s]$
MTR	Mix-Then-Reside Reactor	
Nu	Nusselt Number	$[-]$
ΔP	Pressure loss across reactor length	$[Pa]$
Pr	Prandtl Number	$[-]$
q	Heat Transferred	$[W]$
Q	Volumetric flow rate	$[m^3/s]$
r	Reaction rate	$[mol/s]$
R_c	Radius of Curvature	$[m]$
R_{cond}	Resistance to heat transfer via conduction	$[K/W]$
$R_{contact}$	Resistance to heat transfer via contact between the plates	$[K/W]$
R_{conv}	Resistance to heat transfer via convection	$[K/W]$
R_{ext}	External resistance to heat transfer	$[K/W]$
R_{tot}	Total resistance to heat transfer in the system	$[K/W]$
Re	Reynolds Number	$[-]$
RTC	Residence Time Channel	
T	Temperature	$[°C\ or\ K]$
t	Wall thickness	$[m]$
TG	Tangential Mixer	
u	Superficial velocity of the fluid at the contraction	$[m/s]$
U	Overall heat transfer coefficient	$[W/(m^2\,K)]$
V	Volume	$[m^3]$
w	Contraction width	$[m]$

Greek Symbols

α	Aspect ratio (w/d)	$[-]$
β	1st fitted parameter for Gnielinski-type model	$[-]$
γ	2nd fitted parameter for Gnielinski-type model	$[-]$
ε	Average rate of energy dissipation $(\Delta P/\rho\tau)$	$[m^2/s^3]$
μ	Dynamic viscosity	$[Pa\ s]$
ρ	Density	$[kg/m^3]$
τ	Average residence time	$[s]$

Subscripts

$1,2$	Two different scales
c	Cold stream
DB	Dittus-Boelter
f	Fluid
Gn	Gnielinski
h	Hot stream
HE	Heat exchange
i	Measured at inlet
in	Inner channel side (in this case RTC or MTR side)
LM	Log mean
ME	Mixing Element
o	Measured at outlet
out	Outer channel side (in this case HTF side)
R	Reactor side
rxn	Reaction
s	Conditions at the wall surface
ST	Sieder-Tate
TF	Transfer fluid
tot	Total
w	across the wall

Acknowledgements. The authors would like to thank the Natural Sciences and Engineering Research Council of Canada, including the CREATE program in Continuous Flow Science, and Lonza AG for their financial contribution. Also, Ehrfeld Mikrotechnik BTS is acknowledged for the reactor manufacturing.

3.6. References

[1] N.-T. Nguyen, Z. Wu, Micromixers—a review, J. Micromechanics Microengineering. 15 (2005) R1–R16. doi:10.1088/0960-1317/15/2/R01.

[2] M.N. Kashid, L. Kiwi-Minsker, Microstructured Reactors for Multiphase Reactions: State of the art, Ind. Eng. Chem. Res. 48 (2009) 6465–6485. doi:10.1021/ie8017912.

[3] N. Kockmann, M. Gottsponer, D.M. Roberge, Scale-up concept of single-channel microreactors from process development to industrial production, Chem. Eng. J. 167 (2011) 718–726. doi:10.1016/j.cej.2010.08.089.

[4] V. Kumar, M. Paraschivoiu, K.D.P. Nigam, Single-phase fluid flow and mixing in microchannels, Chem. Eng. Sci. 66 (2011) 1329–1373. doi:10.1016/j.ces.2010.08.016.

[5] N. Kockmann, D.M. Roberge, Scale-up concept for modular microstructured reactors based on mixing, heat transfer, and reactor safety, Chem. Eng. Process. Process Intensif. 50 (2011) 1017–1026. doi:10.1016/j.cep.2011.05.021.

[6] P.S. Lee, S. V. Garimella, Thermally developing flow and heat transfer in rectangular

microchannels of different aspect ratios, Int. J. Heat Mass Transf. 49 (2006) 3060–3067. doi:10.1016/j.ijheatmasstransfer.2006.02.011.

[7] S. Kandlikar, S. Garimella, D. Li, S. Colin, M.R. King, Heat Transfer and Fluid Flow in Minichannels and Microchannels, 2nd ed., Elsevier Ltd., Kidlington, Oxford, 2014. doi:10.1016/B978-0-08-098346-2.00003-X.

[8] I. Rossetti, M. Compagnoni, Chemical reaction engineering, process design and scale-up issues at the frontier of synthesis: Flow chemistry, Chem. Eng. J. 296 (2016) 56–70. doi:10.1016/j.cej.2016.02.119.

[9] P. Plouffe, A. Macchi, D.M. Roberge, From batch to continuous chemical synthesis-a toolbox approach, Org. Process Res. Dev. 18 (2014) 1286–1294. doi:10.1021/op5001918.

[10] P. Barthe, C. Guermeur, O. Lobet, M. Moreno, P. Woehl, D.M. Roberge, et al., Continuous multi-injection reactor for multipurpose production - Part I, Chem. Eng. Technol. 31 (2008) 1146–1154. doi:10.1002/ceat.200800132.

[11] D.M. Roberge, N. Bieler, M. Mathier, M. Eyholzer, B. Zimmermann, P. Barthe, et al., Development of an industrial multi-injection microreactor for fast and exothermic reactions - Part II, Chem. Eng. Technol. 31 (2008) 1155–1161. doi:10.1002/ceat.200800131.

[12] P. Plouffe, M. Bittel, J. Sieber, D.M. Roberge, A. Macchi, On the scale-up of micro-reactors for liquid–liquid reactions, Chem. Eng. Sci. 143 (2016) 216–225. doi:10.1016/j.ces.2015.12.009.

[13] F.P. Incropera, D.P. DeWit, T.L. Bergman, A.S. Lavine, Fundamentals of Heat and Mass Transfer, 7th ed., John Wiley & Sons, Inc., Jefferson City, 2011.

[14] G.L. Morini, Single-phase convective heat transfer in microchannels: A review of experimental results, Int. J. Therm. Sci. 43 (2004) 631–651. doi:10.1016/j.ijthermalsci.2004.01.003.

[15] M.E. Steinke, S.G. Kandlikar, Single-phase liquid heat transfer in microchannels, in: 3rd Int. Conf. Microchannels Minichannels, 2005. doi:10.1115/ICMM2005-75114.

[16] W.M. Kays, M.E.E. Crawford, Convective Heat and Mass Transfer, 4th ed., McGraw-Hill, Boston, 2005.

[17] N. Kockmann, Transport Phenomena in Micro Process Engineering, Springer Berlin Heidelberg, Berlin, Heidelberg, 2008. doi:10.1007/978-3-540-74618-8.

[18] W.R. Dean, Note on the motion of fluid in a curved pipe, London, Edinburgh, Dublin Philos. Mag. J. Sci. 4 (1927) 208–223.

[19] W.R. Dean, The stream-line motion of fluid in a curved pipe, London, Edinburgh, Dublin Philos. Mag. J. Sci. 5 (1928) 673–695.

[20] F. Jiang, K.S. Drese, S. Hardt, M. Kupper, F. Schonfeld, Helical flows and chaotic mixing in curved micro channels, AIChE J. 50 (2004) 2297–2305. doi:10.1002/aic.10188.

[21] F. Schönfeld, S. Hardt, Simulation of helical flows in microchannels, AIChE J. 50 (2004) 771–778. doi:10.1002/aic.10071.

[22] G. Gauthier, P. Gondret, H. Thomé, M. Rabaud, Centrifugal instabilities in a curved rectangular duct of small aspect ratio, Phys. Fluids. 13 (2001) 2831–2834. doi:10.1063/1.1400136.

[23] R.H. Perry, D.W. Green, J.O. Maloney, eds., Perry's Chemical Engineers' Handbook, 8th ed., McGraw-Hill, New York, 2007.

[24] T.. Adams, M.. Dowling, S.. Abdel-Khalik, S.. Jeter, Applicability of traditional turbulent single-phase forced convection correlations to non-circular microchannels, Int. J. Heat Mass Transf. 42 (1999) 4411–4415. doi:10.1016/S0017-9310(99)00102-7.

[25] T.M. Adams, S.I. Abdel-Khalik, S.M. Jeter, Z.H. Qureshi, An experimental investigation of single-phase forced convection in microchannels, Int. J. Heat Mass Transf. 41 (1998) 851–857. doi:10.1016/S0017-9310(97)00180-4.

[26] Haynes International, HASTELLOY® C-22® Alloy, (2015). http://www.haynesintl.com/alloys/alloy-portfolio_/Corrosion-resistant-Alloys/HASTELLOY-C-22-.aspx (accessed September 21, 2016).

[27] McMaster-Carr, Electrically and Thermally Conductive Grease, (2016). http://www.mcmaster.com/#1219k59/ (accessed September 21, 2016).

[28] J. Pátek, J. Hrubý, J. Klomfar, M. Součková, A.H. Harvey, Reference Correlations for Thermophysical Properties of Liquid Water at 0.1 MPa, J. Phys. Chem. Ref. Data. 38 (2009) 21. doi:10.1063/1.3043575.

[29] J.R. Couper, W.R. Penney, J.R. Fair, S.M. Walas, Chemical Process Equipment: Selection and Design, 3rd ed., Elsevier, Waltham MA, 2012.

[30] R. Andreozzi, M. Canterino, V. Caprio, I. Di Somma, R. Sanchirico, Batch salicylic acid nitration by nitric acid/acetic acid mixture under isothermal, isoperibolic and adiabatic conditions, J. Hazard. Mater. 138 (2006) 452–458. doi:10.1016/j.jhazmat.2006.05.104.

[31] B. Ahmed-Omer, D. Barrow, T. Wirth, Effect of segmented fluid flow, sonication and phase transfer catalysis on biphasic reactions in capillary microreactors, Chem. Eng. J. 135 (2008) S280–S283. doi:10.1016/j.cej.2007.07.017.

[32] B. Ahmed, D. Barrow, T. Wirth, Enhancement of reaction rates by segmented fluid flow in capillary scale reactors, Adv. Synth. Catal. 348 (2006) 1043–1048. doi:10.1002/adsc.200505480.

[33] V.D. Parker, Instantaneous rate constants in physical organic chemistry: Application to

acyl transfer reactions of p-nitrophenyl acetate to hydroxide ion, J. Phys. Org. Chem. 19 (2006) 714–724. doi:10.1002/poc.1064.

[34] P. Plouffe, D.M. Roberge, A. Macchi, Liquid–liquid flow regimes and mass transfer in various micro-reactors, Chem. Eng. J. 300 (2016) 9–19. doi:10.1016/j.cej.2016.04.072.

[35] P. Plouffe, D.M. Roberge, J. Sieber, M. Bittel, A. Macchi, Liquid–liquid mass transfer in a serpentine micro-reactor using various solvents, Chem. Eng. J. 285 (2016) 605–615. doi:10.1016/j.cej.2015.09.115.

[36] E. Mielke, D.M. Roberge, A. Macchi, Microreactor mixing-unit design for fast liquid—liquid reactions, J. Flow Chem. 6 (2016) 279–287. doi:10.1556/1846.2016.00026.

[37] J.R. McDonough, A.N. Phan, A.P. Harvey, Rapid process development using oscillatory baffled mesoreactors – A state-of-the-art review, Chem. Eng. J. 265 (2015) 110–121. doi:10.1016/j.cej.2014.10.113.

[38] S.S. Mongeon, D.M. Roberge, M. Bittel, P. Elsner, A. Macchi, Liquid–Liquid Mass Transfer in an Oscillatory-Flow Mesoscale Coil Reactor without Baffles, Org. Process Res. Dev. (2016) acs.oprd.5b00356. doi:10.1021/acs.oprd.5b00356.

4. Conclusions and Future Work

4.1. Conclusions

The "toolbox" developed by Plouffe et al. [1] can be useful in properly selecting a reactor for a broad set of conditions such as reaction rate (fast, moderate, slow) and phase properties (homogenous, liquid-liquid, liquid-gas, gas-solid, etc.). The work presented here provides detailed insight when selecting reactors specifically for fast liquid-liquid reactions, or for highly exothermic reactions, where micro-reactors could be employed to enhance the transport properties of a fluid system.

In section 2, several obstacle-based micro-mixer geometries were investigated with up to four different solvent-pair systems for two different mixer scales. The liquid-liquid systems were visually classified based on some combination of the following flow regimes: slug flow; parallel flow; or drop flow. The drop flow regime has the highest specific area available for interphase mass transfer and is, therefore, ideal for applications in fast liquid-liquid reactions. Using the alkaline hydrolysis of 4-nitrophenyl acetate as a test reaction, the overall volumetric mass transfer coefficient ($K_{org}a$) could be measured analytically. The $K_{org}a$ was plotted vs. the average rate of energy dissipation (ε) to determine the most efficient mixer design (i.e., the mixer with the earliest onset of drop flow). In the flow range of 1-20 mL/min, the novel LL-Triangle micro-mixer design was shown to perform equally well or better in all solvent-pairs investigated than any of the other micro-mixers studied: the Sickle, the LL-Rhombus, and the LL-Empty. The LL-Triangle was most clearly superior to the other geometries at low flow rates for low interfacial tension systems, such as *n-butanol-water*, where the drop flow regime was observed at the lowest energy dissipation, and the unwanted parallel flow regime was avoided altogether.

The same results were seen in a larger scale LL-Triangle where drop flow was achieved for all flow rates studied (10-150 mL/min) in *n-butanol-water*. The overall volumetric mass transfer coefficients were similar to those obtained at equal energy dissipations in the smaller scale in the drop flow regime; confirming the "$3/7^{th}$" scale-up rule. Thus, the LL-Triangle is an excellent tool for the purpose of process development and scale-up of novel fast liquid-liquid reactions.

Heat transfer properties were then examined in section 3 for a FlowPlate® system by Ehrfeld Mikrotechnik BTS, using both non-reactive and reactive techniques. In the non-reactive system

in section 3.1, the Nusselt Number was fit to a Gnielinski-type model for a serpentine rectangular channel for $400 < Re < 2000$. The use of a transitional model (from laminar to turbulent flow) was deemed appropriate for such low Re due to the formation of chaotic eddies from the curvature (Dean vortices). In addition to understanding the internal heat transfer coefficients, the external resistances to heat transfer were tested; specifically, the heat transfer fluid (HTF) flow rate and the contact resistance between the HTF plate and reactor plate. The largest contributor to the resistance of heat transfer was shown to be the contact resistance, which could significantly reduce the external resistance (by approximately 70%) using a silver-based thermal paste.

The synthesis of methyl 2-oxobutanoate using dimethyl-oxalate and the Grignard reagent ethylmagnesium chloride was then presented in section 3.2 as a test reaction to differentiate localized heat transfer characteristics in various micro-reactors. The reaction's fast reaction kinetics, high exothermicity, and the increased selectivity for the desired product at lower temperatures allow for a semi-quantitative comparison of hotspot formation in different plate reactors (e.g., various micro-mixer geometries, materials, injection ports, and channel scales) when comparing total yields. A multi-injection approach was the most effective method for reducing the magnitude of the hotspot, thereby increasing the reaction yield. Additionally, micro-mixers with higher specific area had higher yields due to increased wall-to-fluid heat transfer.

Finally, section 3.3 considered four case studies which calculated the maximum channel diameter that would allow sufficient heat removal based on the overall heat transfer coefficients found experimentally (in section 3.1) and the fourth Damköhler number. The first case involved the Grignard reaction from section 3.2, while the second case considered an auto-catalytic nitration reaction. The third and fourth cases looked at the kinetics of the mass transfer limited hydrolysis reaction (used in section 2) for *n-butanol-water* and *toluene-water* systems, respectively. This section was presented as a tool (to add to the toolbox from Plouffe et al.) to select suitable channel dimensions to ensure adequate heat transfer properly.

4.2. Future Work

While the work presented in this thesis has highlighted a novel micro-mixer geometry for liquid-liquid reactions as well as various techniques for understanding heat transfer in micro-reactor

systems, several prospects for extending the scope of this project remain. The following studies are recommended:

- Attempt other multiphase flow in the LL-Triangle micro-mixer. Determine if it can be used to control the particle size distribution of a precipitation reaction (without plugging), or to disperse a gas in a liquid.
- Use a high-speed, high-resolution camera to fully understand the various flow regimes in the micro-mixers for different interfacial tensions and how dead zones (if any) form.
- Perform tracer experiments to obtain residence time distributions in the different reactors to determine if the reactors can be considered truly “plug flow”.
- Perform multi-phase heat transfer experiments with the mixer geometries from section 2 to study the effect of flow regime on the wall-to-fluid heat transfer.
- Obtain the kinetic data for the Grignard reaction from section 3.2 to simulate and detail the effect of flow rate on the product yield. This would allow for the fully quantitative analysis of hotspot formation in various micro-reactors.

4.3. References

[1] P. Plouffe, A. Macchi, D.M. Roberge, From Batch to Continuous Chemical Synthesis—A Toolbox Approach, Org. Process Res. Dev. (2014). doi:10.1021/op5001918.